frontiers | Frontiers in Earth Science

TYPE Original Research
PUBLISHED 27 March 2025
DOI 10.3389/feart.2025.1501498

Check for updates

OPEN ACCESS

EDITED BY
Eric Josef Ribeiro Parteli,
University of Duisburg-Essen, Germany

REVIEWED BY
Mohammad Azarafza,
University of Tabriz, Iran
Jeffrey Perez,
Philippine Institute of Volcanology and Seismology, Philippines

*CORRESPONDENCE
Chong Xu,
xc11111111@126.com,
chongxu@ninhm.ac.cn

RECEIVED 25 September 2024
ACCEPTED 05 March 2025
PUBLISHED 27 March 2025

CITATION
Wang Q and Xu C (2025) What are the spatial distribution characteristics of the 4417 landslides in Minhe County, Qinghai Province, China?
Front. Earth Sci. 13:1501498.
doi: 10.3389/feart.2025.1501498

COPYRIGHT
© 2025 Wang and Xu. This is an open-access article distributed under the terms of the Creative Commons Attribution License (CC BY). The use, distribution or reproduction in other forums is permitted, provided the original author(s) and the copyright owner(s) are credited and that the original publication in this journal is cited, in accordance with accepted academic practice. No use, distribution or reproduction is permitted which does not comply with these terms.

What are the spatial distribution characteristics of the 4417 landslides in Minhe County, Qinghai Province, China?

Qinxia Wang[1] and Chong Xu[1,2]*

[1]National Institute of Natural Hazards, Ministry of Emergency Management of China, Beijing, China, [2]Key Laboratory of Compound and Chained Natural Hazards Dynamics, Ministry of Emergency Management of China, Beijing, China

Landslide relic inventories serve as essential data for geological disaster investigations and risk assessments. Using a previously developed landslide relic inventory for Minhe County, Qinghai Province, this study employs landslide number density (LND) and landslide area percentage (LAP) to thoroughly investigate the spatial distribution characteristics of landslides in the region. Utilizing a GIS platform, we selected ten factors for in-depth analysis, including elevation, slope aspect, slope gradient, relief degree of land surface, distance to faults, lithology, land use type, distance to rivers, rainfall, and NDVI. The results show that at least 5,517 landslide relics have developed in Minhe County, with a total landslide coverage area of 434.43 km^2. These landslides are mainly distributed in regions with elevations of 2000–2100 m, slope gradients of 15°–25°, Neogene strata, grassland, and within 0–2 km of rivers. Both slope and aspect are the most significant factors influencing the landslide relics in Minhe County. The findings of this study contribute to a better understanding of the development characteristics and spatial distribution of landslides in the Huangshui River Basin and provide valuable data support for future landslide assessments and disaster prevention efforts.

KEYWORDS

huangshui river basin, upper yellow river, landslide inventory, google earth, visual interpretation, spatial analysis

1 Introduction

Landslides are a common geological hazard worldwide (Li et al., 2021a; Petley, 2012; Qiu et al., 2018; Wang et al., 2021; Li et al., 2021b). Many landslides are characterized by large scale, high frequency, and rapid occurrence, often resulting in catastrophic consequences that pose significant threats to human life, property, and socio-economic development (Lin et al., 2008; Wang et al., 2018; Ma et al., 2024c; Shao et al., 2024b; Nanehkaran et al., 2022). China is one of the countries most severely affected by landslides worldwide (Xue et al., 2023; Ma et al., 2023d; Zhao et al., 2024). Between 1950 and 2016, China recorded 1,911 fatal landslides, resulting in 28,139 deaths (Froude and Petley, 2018). These statistics highlight the devastating impact of landslide hazards. Therefore, understanding the mechanisms behind landslides and conducting research on landslide prevention are crucial (Huang et al., 2023). Current research on landslides primarily focuses on landslide inventories (Valenzuela et al., 2017; Wang et al., 2022), spatial distribution patterns (Frattini and Crosta, 2013; Korup, 2005; Shao et al., 2024a), susceptibility assessments

(Cui et al., 2022; Liu et al., 2022; Cemiloglu et al., 2023; Ali et al., 2021), hazard evaluation (Ma et al., 2022; Shao et al., 2023c), numerical simulations (Cui et al., 2021; Xia et al., 2021), stability analysis (Wu et al., 2023), and monitoring and early warning systems (Yin et al., 2010a). Among these, constructing landslide inventories is a fundamental basis for conducting further research (Zhao et al., 2023). Landslide inventories typically provide detailed information on the location, type, and spatial distribution of landslides in a given region (Guzzetti et al., 2012; Piacentini et al., 2018; Wieczorek, 1984; Xu, 2015), which is essential for subsequent studies on their spatial patterns and risk assessment.

Building on the establishment of landslide inventories, scholars both domestically and internationally have conducted extensive studies on the spatial distribution patterns of landslides, utilizing a variety of methods such as field surveys, historical aerial imagery analysis (Kubwimana et al., 2021), satellite imagery and the integration of InSAR technology (Chen et al., 2022). By analyzing these spatial distribution characteristics, we can effectively identify high-risk landslide areas and provide scientific support for disaster prevention efforts. Moreover, to better understand the causes of landslides, researchers often explore vital factors influencing their occurrence. Landslides are typically the result of the combined effects of various factors, including geological, geomorphological, and climatic conditions (Huang et al., 2022). Currently, there is no consensus on the selection of factors that influence landslides in academic research. Most studies use eight common factors: elevation, slope, aspect, lithology, distance to faults, distance to rivers, rainfall, and land use. Additionally, depending on the region and purpose of the study, scholars may introduce additional influencing factors to enrich their findings. For example, in studies of rainfall-induced landslides, researchers have included factors such as the topographic wetness index (TWI) (Xie et al., 2023), the relief degree of land surface (Ma et al., 2023c), the normalized difference vegetation index (NDVI) (Li et al., 2024a). For earthquake-induced landslides, common additional factors include the topographic position index (TPI) (Chen et al., 2023c), peak ground velocity (PGV) (Ma et al., 2023a), peak ground acceleration (PGA) (Ma et al., 2024d; Shao et al., 2022), and earthquake intensity (Shao et al., 2023b; Xiao et al., 2023). In studies on landslide relics, factors such as curvature (Naseer et al., 2021), soil type (Quan et al., 2014), stream power index (SPI) (Chen et al., 2023b), and distance to roads (Bui et al., 2012) have been introduced. Although current research offers valuable insights into the spatial distribution patterns and triggering factors of landslides, studies on landslides in China remain incomplete, and many landslide-prone areas still require further exploration.

The Huangshui River Basin, situated in the upper reaches of the Yellow River, lies in the transition zone between the first and second steps on the northeastern edge of the Qinghai-Tibet Plateau. This region is characterized by intense tectonic activity and complex lithology, with large landslides widely distributed (Zhang et al., 2023). The hilly areas in the middle and lower reaches of the basin are highly prone to geological disasters, both within Qinghai Province and across the country (Cui et al., 2015; Zhou et al., 2002). According to surveys conducted by the Qinghai Hydrology and Environmental Engineering Department, loess landslides in the Huangshui River Basin have caused 26 deaths, destroyed 1,007 houses, and resulted in direct economic losses exceeding 4 million yuan (Zhou et al., 2013). In recent years, significant progress has been made in the study of landslide spatial distribution patterns and causal mechanisms in the upper reaches of the Yellow River (Li Z. et al., 2024; Tu et al., 2023). Existing research has primarily focused on critical parameters such as slope gradient, geotechnical structure, and stratigraphic chronology (Zhang and Liu, 2010; Zhao et al., 2025; Huang et al., 2022; Li Z. et al., 2024), offering in-depth insights into the developmental mechanisms and spatial characteristics of landslides in this region. However, despite substantial advancements, the spatial heterogeneity and evolutionary processes of landslide hazards across different subregions remain insufficiently explored and require further refinement. The Huangshui River, one of the most significant tributaries of the upper Yellow River, flows through a geologically complex and tectonically active landscape. This river basin also constitutes the political, economic, and cultural center of Qinghai Province, where its geographical and environmental conditions exert profound influences on regional socioeconomic development and ecological security. Among the areas within this basin, Minhe County, located in the lower reaches of the basin, has emerged as a high-risk area for landslide hazards due to its highly undulating topography, loosely consolidated geotechnical materials, and the compounded effects of multiple contributing factors. Building upon prior research, this study utilizes a systematically compiled landslide inventory for Minhe County to analyze the spatial distribution characteristics of landslides. Ten key influencing factors were selected, including elevation, aspect, slope gradient, topographic relief, distance to faults, lithology, land use type, distance to rivers, precipitation, and the NDVI. Through a comprehensive spatial analysis, we investigated the relationships between these factors and landslide occurrence, providing preliminary insights into the primary controlling mechanisms of landslide activity in the region. This research not only enhances the understanding of landslide formation processes and evolutionary patterns in Minhe County but also provides a robust scientific foundation for regional disaster risk assessment, infrastructure safety planning, and land-use optimization. Ultimately, the findings contribute to the development of an integrated disaster prevention and mitigation framework, supporting the long-term sustainability and resilience of the region against geohazards.

2 Study area overview

Minhe Hui and Tu Autonomous County (referred to as Minhe County) is located in the eastern part of Haidong City, Qinghai Province, China (coordinates: 102°26′–103°04′E, 35°45′–36°26′N), covering a total area of 1,890 square kilometers (Figure 1). Minhe County lies in the transition zone between the Loess Plateau and the Qinghai-Tibet Plateau, featuring a complex terrain with deep ravines and overlapping mountain ranges. The topography is generally higher in the northwest and lower in the southeast, with the southwestern part dominated by high mountains. The Huangshui and Yellow Rivers flow from west to east through the northern and southern parts of the county, forming the Huangshui and Yellow River valleys. The region experiences a temperate, plateau continental arid climate with an average annual temperature of 9°C.

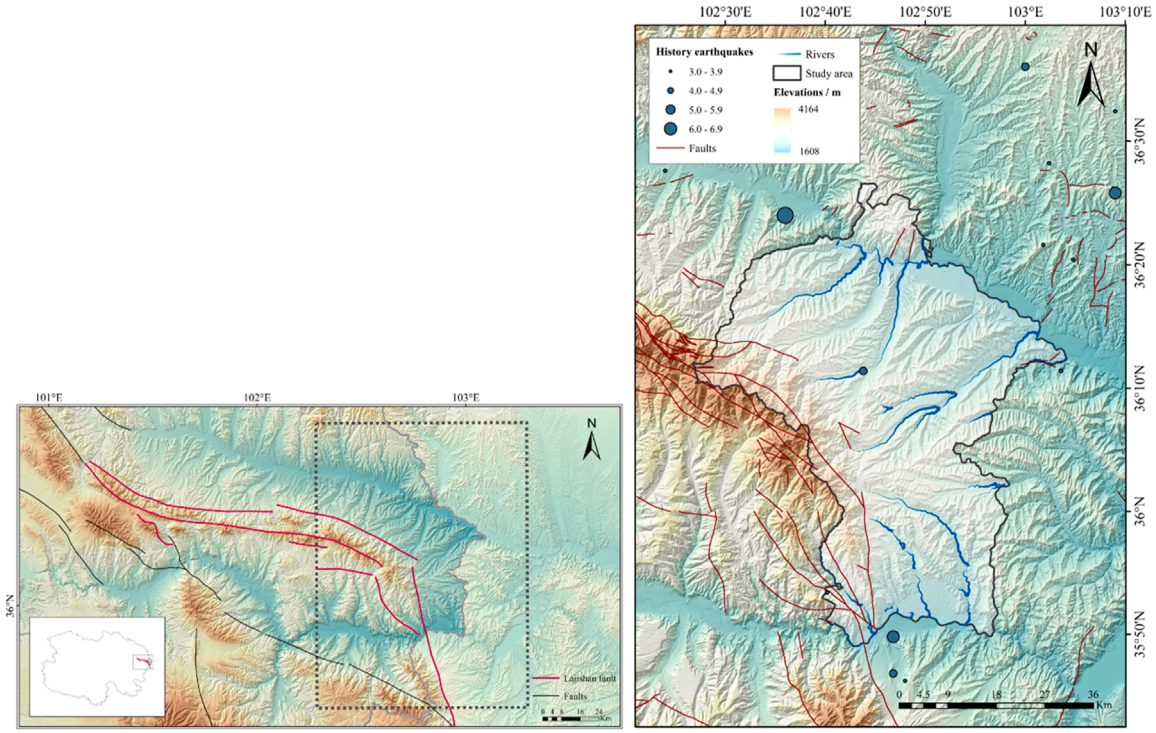

FIGURE 1
Overview of the study area.

Precipitation is unevenly distributed throughout the year, mainly concentrated between May and September, with an average annual rainfall of approximately 292.2 mm.

Minhe County is situated between the South Qilian and North Qilian geosynclinal fold belts and primarily falls within the eastern extension of the Central Qilian fold belt. The main geological structures include the Sangjia-Guantan thrust fault, the Baijiasi-Zhaojia thrust fault, and the Zhaerleng-Keer'ao thrust fault. Stratigraphically, the region is dominated by formations from the Quaternary, Paleogene, Neogene, and Cambrian periods. The Quaternary loess, along with the Paleogene and Neogene red beds, constitutes the main landslide-prone units in the region (Kou et al., 2017).

According to the earthquake catalog published by the China Seismic Network (CSN), the earthquake data for the study area are presented in Supplementary Table S1.

3 Data and methods

3.1 Selection and processing of influencing factors

3.1.1 Selection of influencing factors

To analyze the spatial distribution of landslides in Minhe County, we referenced studies conducted by previous scholars (Wang et al., 2022). Landslide number density (LND) and landslide area percentage (LAP) were selected as key indicators for measuring the spatial distribution of landslides in the study area. LND describes the concentration of landslides, representing the number of landslides per square kilometer (Equation 1). LAP, on the other hand, represents the scale of landslides, expressed as the percentage of the landslide area relative to various influencing factors (Equation 2).

$$LND = \frac{Landslide\ number}{Classified\ area\ of\ variable\ I} \quad (1)$$

$$LAP = \frac{Landslide\ area}{Classified\ area\ of\ variable\ I} \quad (2)$$

By comparing the number of landslides and the areas affected under different influencing factors, we can analyze the spatial distribution patterns of landslides. This method is regarded as the simplest and most fundamental approach for studying landslide spatial distribution (Cui et al., 2024). We used a GIS platform for this analysis. By reclassifying the raster layers of each influencing factor and extracting the values for multiple factors at each landslide point, we determined the number and area of landslides within each factor category. Based on these data, we calculated the LND and LAP values for each category and conducted an in-depth investigation of landslide spatial distribution patterns.

In this study, considering the availability of existing data and drawing on previous research, we selected 10 influencing factors for analysis. These include four topographic factors (elevation, slope aspect, slope gradient, Relief degree of land surface), three geological and geomorphological factors (distance to faults, lithology, land use), and three hydrological and ecological factors (distance to rivers, rainfall, NDVI).

3.1.2 Processing of influencing factors

For the convenience of subsequent calculations in our study, we processed the raw data of the influencing factors to transform them into a format suitable for machine learning model analysis. In this study, two types of factor data need to be processed and converted: continuous factors and categorical factors.

For continuous factors, such as DEM, slope, rainfall, and topographic relief, we discretized the data. Discretization involves dividing the numerical range of continuous factors into several intervals, with each interval representing a specific factor level. For example, for DEM values (which represent the elevation of the region), we typically start with the lowest value in the area and divide it into intervals of 100 m, creating multiple levels. The methods used for discretization include equal interval classification and natural breaks classification. Discretization helps simplify the model analysis process, making the model easier to understand and interpret.

For categorical factors, such as lithology and land type, we convert their attribute information into numerical format by assigning specific values, so that the model can accurately identify and analyze the influence of different categories. For example, the lithology factor contains information about various geological ages, and we can convert this information into numerical values (such as assigning values like 1, 2, 3) to facilitate further analysis in the model.

3.1.3 Correlation of influencing factors

We selected the Pearson Correlation Coefficient (PCC) to further investigate the correlations between the influencing factors. The Pearson Correlation Coefficient is a statistical measure that quantifies the degree of linear correlation between two variables (Ullah et al., 2024). The value of the Pearson Correlation Coefficient ranges from −1 to 1. A positive r_{xy} indicates a positive correlation between the two factors, while a negative r_{xy} indicates a negative correlation. If r_{xy} is close to 0, it suggests that there is almost no linear correlation between the two factors.

When the absolute value of the correlation coefficient between two factors exceeds 0.7, a strong correlation is considered to exist between them (Hong et al., 2020; Qin et al., 2021). By calculating the Pearson Correlation Coefficients between the influencing factors, we can effectively identify factor pairs with strong correlations and selectively retain one factor from such pairs, thereby avoiding interference between factors and addressing multicollinearity issues (Selamat et al., 2024). Specifically, the formula for calculating the Pearson Correlation Coefficient is as follows:

$$r_{xy} = \frac{\sum_{i=1}^{n}\left(X_i - \overline{X}\right)\left(Y_i - \overline{Y}\right)}{\sqrt{\sum_{i=1}^{n}\left(X_i - \overline{X}\right)^2} \times \sqrt{\sum_{i=1}^{n}\left(Y_i - \overline{Y}\right)^2}}$$

Where:

R = Correlation Coefficient.

X_i = Values of x-variable.

$\overline{X}$ = mean of x-variable.

Y_i = Values of y-variable.

$\overline{Y}$ = mean of y-variable.

3.1.4 Importance of influencing factors

Variable Importance Measure (VIM) is a quantitative method used to describe the contribution of each feature to classification or regression tasks. In this study, we utilize the Random Forest (RF) model to calculate the relative importance of influencing factors.

Random Forest is an ensemble learning method introduced by Breiman (2001). It works by constructing multiple decision trees and combining their predictions to improve the accuracy of data analysis and forecasting (Cutler et al., 2012). RF models generally exhibit high predictive accuracy (Chowdhury et al., 2024) and are capable of effectively analyzing data with non-linear relationships, collinearity, and interactions. Additionally, Random Forest not only provides prediction results but also assigns relative importance scores to each variable, making it a widely used and effective tool for evaluating feature importance. In the RF model, feature importance is determined by evaluating the contribution of each feature to the prediction results during the model training process. These importance scores reflect the relative influence of each feature within the model, helping us identify which features have a greater impact on the subsequent susceptibility evaluation results. Therefore, feature importance assessment not only improves the interpretability of the model but also provides a critical basis for further feature selection and model optimization.

3.2 Data sources

The data and sources used in this study are presented in Supplementary Table S2. We clipped the layers of each factor to fit the study area and applied the Universal Transverse Mercator (UTM) projection within the WGS84 coordinate system. The data were resampled to a uniform raster resolution of 12.5 m × 12.5 m. The Digital Elevation Model (DEM), with a resolution of 12.5 m × 12.5 m, was primarily used to extract elevation, slope, aspect, and Relief degree of land surface.

3.3 Landslide data

An accurate and comprehensive landslide inventory is essential for subsequent research, risk assessment, prediction, and disaster management (Du et al., 2020; Wang et al., 2022). In recent years, an increasing number of scholars have focused on constructing landslide relic inventories. For example, using high-resolution remote sensing imagery, scholars have developed landslide inventories for major mountain ranges in China, such as the Yin Mountains (Sun et al., 2024), Taihang Mountains (Zhang et al., 2024), and Qinling Mountains (Feng et al., 2024). Additionally, relatively complete inventories have been created for landslide-prone regions like the Loess Plateau (Peng et al., 2019) and the Qinghai-Tibet Plateau (Wang W. et al., 2024). However, no comprehensive landslide relic inventory has yet been established for Minhe County, the area selected for this study.

In response to this gap, we previously constructed the most comprehensive landslide inventory to date for Minhe County

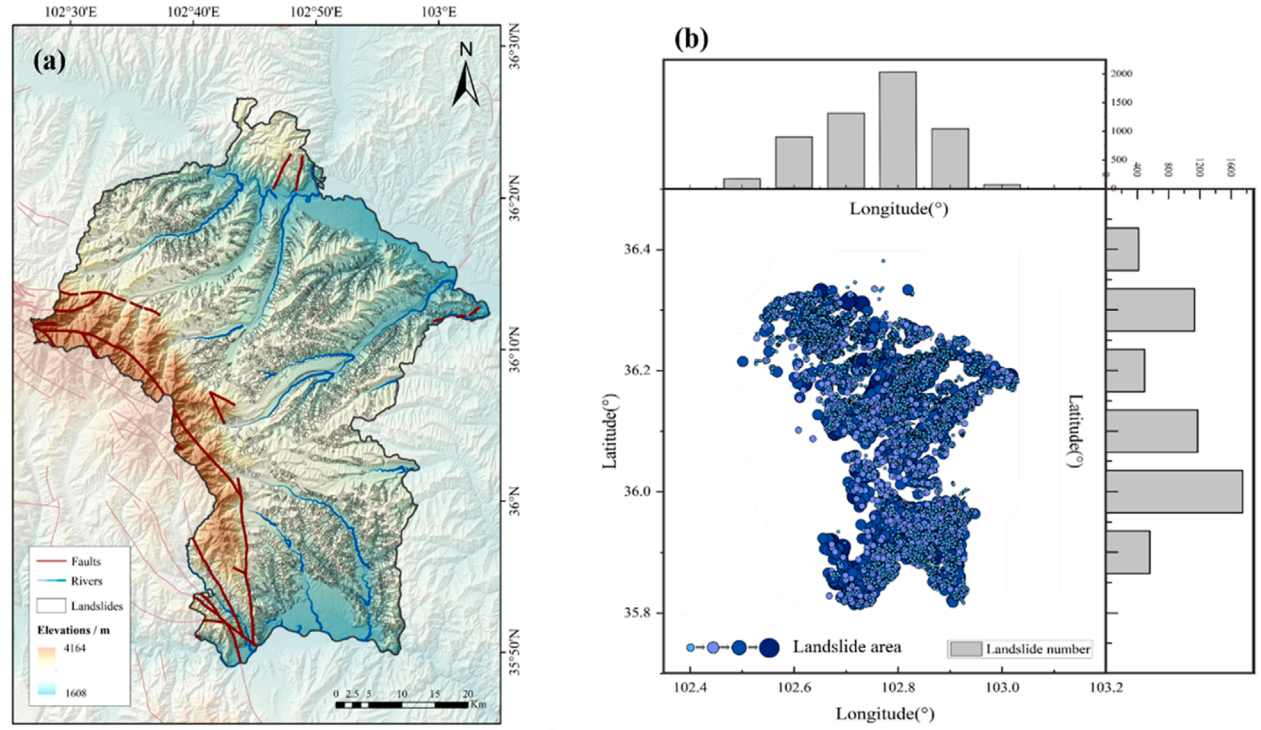

FIGURE 2
(a) Overall spatial distribution of landslides in Minhe County; **(b)** Distribution of landslides of varying magnitudes across different latitudes and longitudes.

(Wang Q. et al., 2024), which serves as the data source for this study. A total of 5,517 landslide relics were identified in the Minhe region, covering a total area of 434.43 km^2, approximately 22.98% of the county's area. The overall distribution of landslides is shown in Figure 2a. The largest single landslide covers an area of 1.62 × 10^6 m^2, while the smallest measures 880.22 m^2, with an average landslide area of 78,743.04 m^2. Statistics indicate that there are 437 landslides with an area smaller than 10,000 m^2, accounting for approximately 7.92% of all landslides. Additionally, 2,547 landslides have an area between 10,000 m^2 and 50,000 m^2, accounting for 46.17% of the total. Moreover, there are 1,318 landslides with an area between 100,000 m^2 and 500,000 m^2, and 1,141 landslides with an area between 500,000 m^2 and 1,000,000 m^2, representing 23.89% and 20.68% of the total, respectively. There are also 74 large landslides with areas exceeding 1 × 10^6 m^2.

As shown in the landslide distribution map, landslide features are widely distributed throughout Minhe County, except in the high-altitude areas in the west and small parts of the northern and southern regions. Additionally, a significant number of landslides are concentrated along the tributaries of the Huangshui and Yellow Rivers, with denser distributions around river bends. Figure 2b illustrates the geographical distribution of landslides of different sizes. The map clearly shows that small landslides are concentrated in the northwest, east, and southeast regions of the county, while larger landslides are primarily located in the northern and southwestern parts.

4 Results

4.1 Spatial distribution of landslides

Using landslide data from previous work, we utilized a GIS platform and applied the Kernel Density method with a 2 km search radius to generate landslide point density and landslide area percentage maps for Minhe County (Figures 3a,b). The results show that the maximum point density in the region is 13.17 km^{-2}, and the maximum area percentage is 87.38%. The spatial distribution of areas with high area percentages largely coincides with those of high point densities, though some regional differences exist. For instance, in the southwestern part of the county, particularly in Xinger Township and Guanting Town, the landslide area percentage is more prominent compared to point density, suggesting that landslides in these areas tend to be larger in scale. In contrast, in the northwestern part of the county, near Xinmin Township and Songshu Township, the landslide point density is more pronounced, indicating a higher number of landslides, though these tend to be smaller in size.

4.2 Analysis of influencing factors

4.2.1 Topographic factors

The elevation of the landslide-affected areas ranges from 1,686 m to 3,565 m. We divided the elevation into 15 intervals, starting from 1,600 m, with each interval spanning 100 m. The statistical results

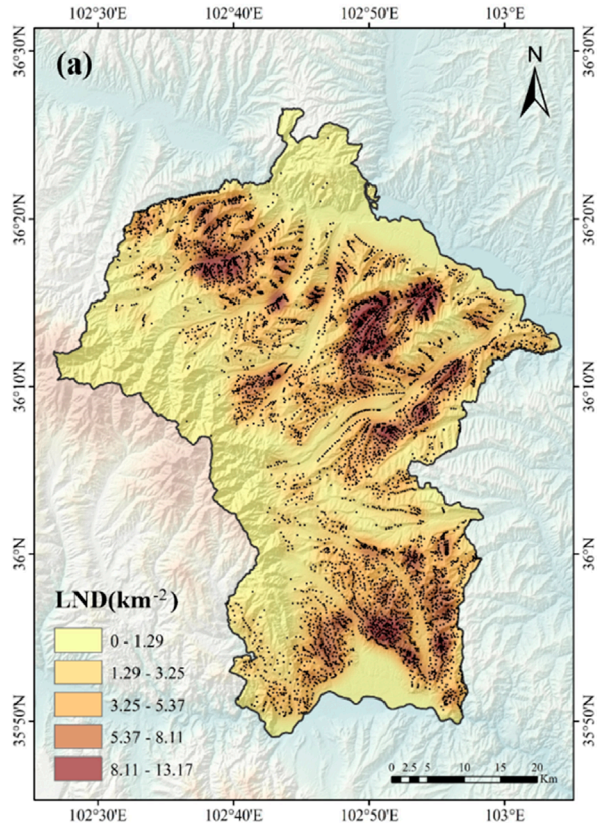

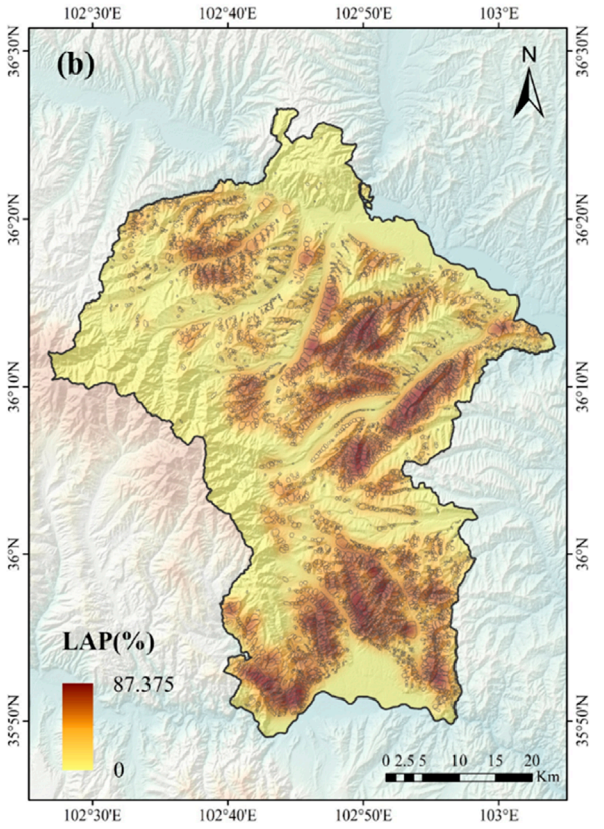

FIGURE 3
Landslide density map. **(a)** Point density map; **(b)** area density map.

are shown in Figure 4. In the 2,000–2,100 m interval, the LND and LAP reach their maximum values of 5.798 km^{-2} and 39.23%, respectively, indicating that both the number of landslides and the total landslide area in this range are significantly greater than in other intervals. A total of 1,122 landslides occurred in this interval, covering an area of 75.91 km^2, accounting for 20.35% of the total number of landslides and 39.23% of the total landslide area.

The slope range of the study area is 0°–78.59°, but the maximum slope within the landslide-affected areas is 59.86°. Therefore, we only considered slopes in the 0°–60° range, divided into intervals of 5°. The results are shown in Figure 5. In the 15°–20° slope range, LAP peaks at 29.84%, while LND reaches its secondary peak at 3.45 km^{-2}. Conversely, in the 20°–25° slope range, LND reaches its peak at 3.88 km^{-2}, while LAP reaches its secondary peak at 28.94%.

Slopes with different orientations receive varying amounts of solar radiation, leading to significant differences in vegetation cover, soil conditions, and evaporation rates (Ma et al., 2024a). In areas with stronger solar radiation, higher evaporation reduces soil moisture, making the soil more prone to weathering, which increases the risk of landslides. The results (Figure 6) indicate that landslides in Minhe County are predominantly concentrated on slopes facing northeast, northwest, west, east, and north, with the northeast-facing slopes covering an area of 54.17 km^2. Both LND and LAP reach their peak values on west-facing slopes, at 3.77 km^{-2} and 30.78%, respectively. On northwest-facing slopes, LND and LAP reach secondary peak values, at 3.39 km^{-2} and 27.88%, respectively.

Relief degree is one of the key parameters in geomorphology, used to describe and reflect the macro features of a region's surface topography. It refers to the difference in elevation between the highest and lowest points within a specific area. Previous studies have shown that the greater the relief degree, the higher the likelihood of landslide occurrence (Wang et al., 2010). The relief degree in Minhe County ranges from 4 to 530, but in the landslide-affected areas, the minimum value is 51 and the maximum value is 453. Therefore, we divided the relief degree into intervals of 50, starting from 50. Due to the smaller number of data points above 250, values between 250 and 413 were merged into a single interval, resulting in five total relief degree intervals. The spatial and numerical distribution of these intervals is shown in Figure 7. As can be seen from the figure, most landslides are distributed in the 100–150 relief degree interval, covering an area of 173.29 km^2, accounting for 41.22% of the total landslide area. The second largest landslide distribution occurs in the 150–200 interval, but the LND and LAP values reach their peak in this interval, at 5.05 km^{-2} and 33.96%, respectively.

4.2.2 Geological and geomorphological factors

The distance between landslide occurrence points and faults in the study area ranges from 0 to 21,204 m. Considering that faults located more than 18 km away have a limited impact on landslides, we combined all distances beyond 18 km into one category, while setting intervals of 3 km for the remaining distances. The statistical results are shown in Figure 8. It is evident that although the landslide

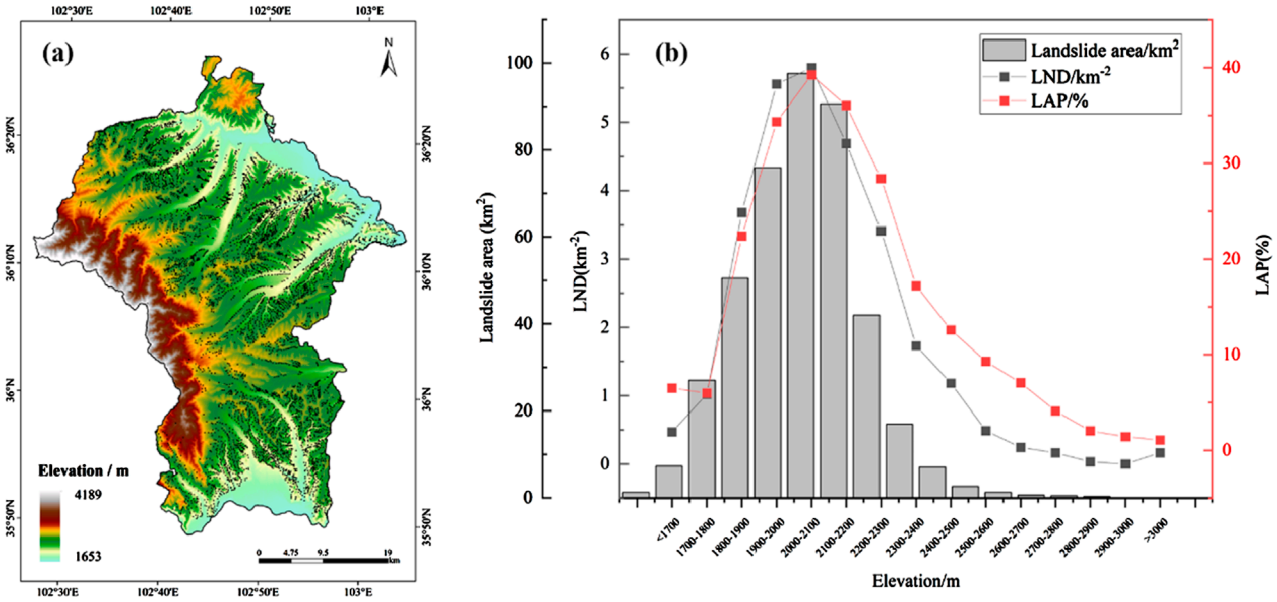

FIGURE 4
Relationship between elevation and landslide distribution. **(a)** Elevation distribution in the study area. **(b)** Statistics of landslide indicators in the elevation intervals.

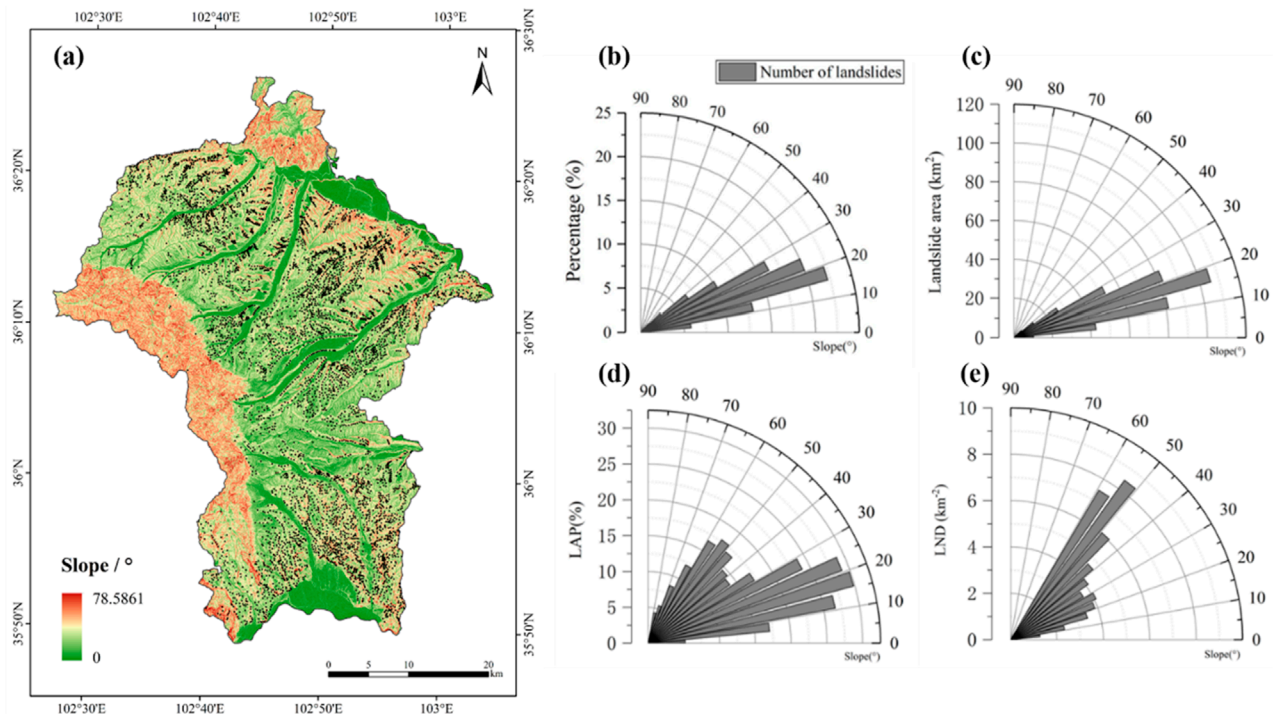

FIGURE 5
Relationship between slope and landslide distribution. **(a)** Slope distribution in the study area. **(b–e)** Statistics of landslide indicators in the slope intervals.

area percentage is highest within the 0–3 km range from faults, the LAP and LND values are the lowest, at only 1.04 km^{-2} and 2.23%, respectively. The LAP and LND values reach their peak in the 12–15 km range, at 4.88 km^{-2} and 6.29%, respectively.

The oldest stratigraphic units in the study area date back to the Early Paleozoic Cambrian period, while the youngest units consist of Quaternary Holocene alluvium and Late Pleistocene glacial deposits, along with other types of sedimentary deposits. Due to the

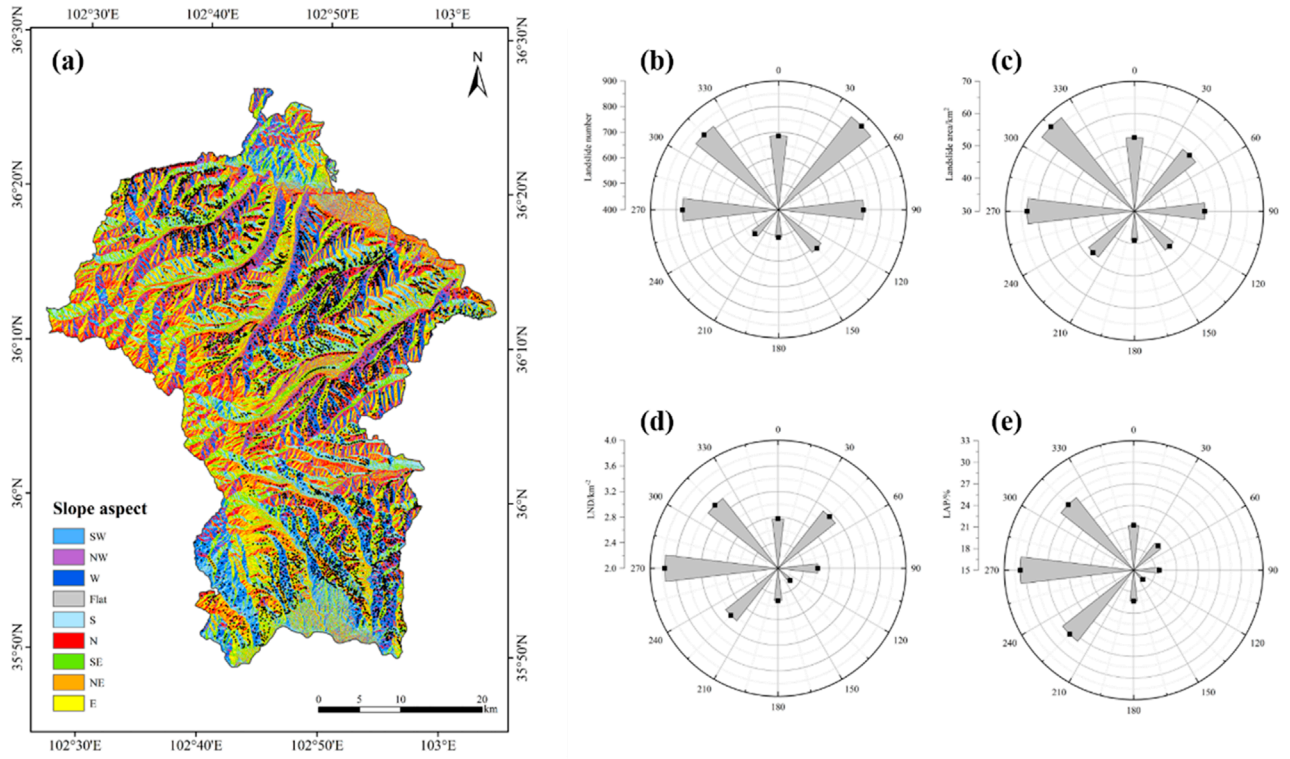

FIGURE 6
Relationship between aspect and landslide distribution. **(a)** Aspect distribution in the study area. **(b–e)** Statistics of landslide indicators in the aspect intervals.

complex lithology, the stratigraphic sections were categorized based on geological age. The statistical results are presented in Figure 9. These results show that the Neogene (N) and Paleogene (E) units exhibit significantly higher LAP and LND values compared to other strata. The Neogene units display the highest LND and LAP values, reaching 4.74 km^{-2} and 42.89%, respectively, while the Paleogene units rank second, with LND at 4.20 km^{-2} and LAP at 32.02%.

The study area has diverse land types, including cropland, grassland, forest land (evergreen broadleaf forest, deciduous broadleaf forest, evergreen coniferous forest), shrubs, grasslands, wetlands, bare land, artificial surfaces, water bodies, and glaciers/snow. However, landslides only occur in seven types of land cover: cropland, grassland, forest land (deciduous broadleaf forest and evergreen coniferous forest), bare land, herbaceous-covered areas, and sparsely vegetated areas. The land use summary is presented in Figure 10. Notably, compared to other land use types, grassland shows the highest LND and LAP values, at 4.23 km^{-2} and 27.39%, respectively. Cropland follows with LND and LAP values of 2.58 km^{-2} and 22.95%, respectively.

4.2.3 Hydrological and ecological factors

The study area is located in the Huangshui Valley, with the Yellow River and Huangshui River flowing through it, making rivers widely distributed. The farthest landslide from a river in the study area occurred at a distance of 8,128 m. Given that only two landslides occurred more than 8 km from a river, we divided the distances into five intervals of 2 km each. The statistical results are shown in Figure 11. As seen from the figure, the area of each interval decreases with increasing distance from the river. Simultaneously, both the LND and LAP values decrease as the distance from the river increases, with both reaching their peak in the 0–2 km interval at 2.55 km^{-2} and 21.62%, respectively.

The maximum annual average rainfall in the study area is 482.9 mm, while the minimum is 151.4 mm. In landslide-affected areas, the maximum annual average rainfall is 324.3 mm. Therefore, starting from 150 mm, we divided the rainfall into intervals of 50 mm, resulting in four categories. The statistical results are shown in Figure 12. The figure clearly indicates that landslide areas are primarily concentrated in the 150–200 mm rainfall interval, followed by the 300–350 mm interval. However, the LND and LAP peak in the 250–300 mm interval, at 4.03 km^{-2} and 27.28%, respectively. Both values show an increasing trend before this interval, followed by a decline.

The NDVI index in the study area ranges from −0.2006 to 0.9989, while the NDVI values within the landslide-affected areas fall between 0.1313 and 0.959. Based on this, we set 0 as the starting point, with an interval increment of 0.2, resulting in five categories. The statistical results are shown in Figure 13. In the 0.4–0.6 interval, LND and LAP reach their peak values at 3.62 km^{-2} and 27.16%, respectively. The second highest values for LND and LAP occur in the 0.2–0.4 interval, at 3.29 km^{-2} and 25.20%, respectively.

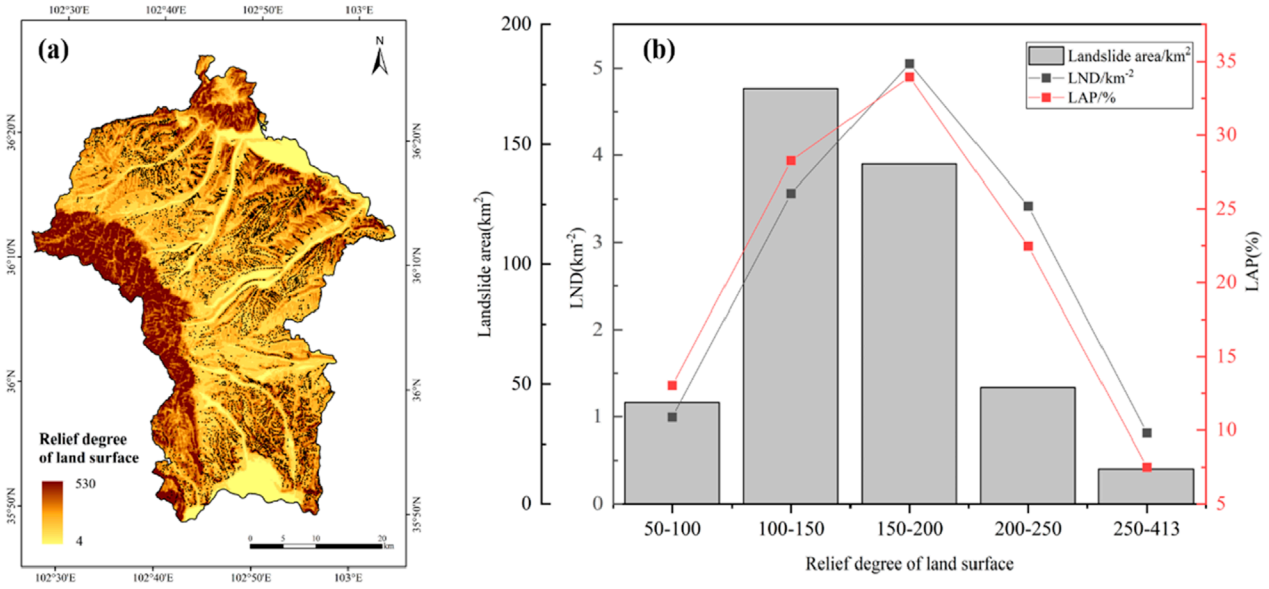

FIGURE 7
Relationship between relief degree and landslide distribution. **(a)** Distribution of relief degree in the study area;**(b)** Statistics of landslide indicators in the relief degree intervals.

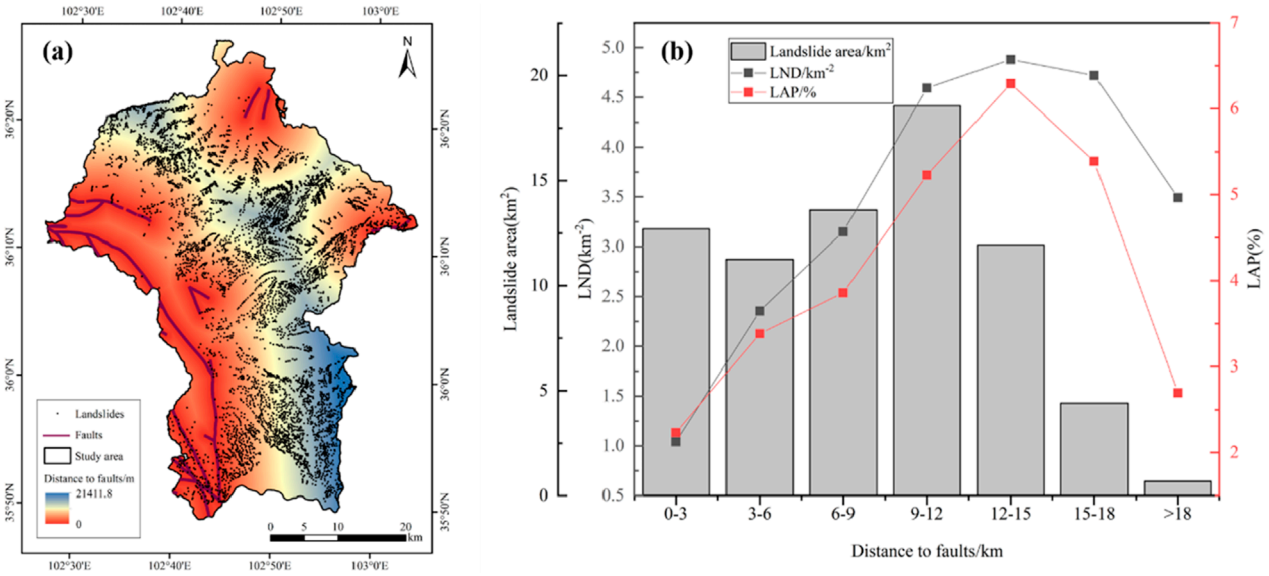

FIGURE 8
Relationship between fault distance and landslide distribution. **(a)** Spatial distribution of faults and landslides within the study area. **(b)** Statistical distribution of landslide occurrences across different distance intervals from faults.

4.3 Correlation and importance analysis of influencing factors

To avoid collinearity issues among the factors, this study conducted a correlation analysis of the 10 factors using the Pearson correlation coefficient. As shown in Figure 14, the absolute values of the correlations between all factors are below 0.7, indicating that there is no collinearity among them. Therefore, the factors are suitable for input into the model for further training.

Based on the analysis results from the Random Forest model, this study systematically ranks the importance of the influencing factors. The results show that slope (0.43428) and aspect (0.38838) have the most significant impact on the landslide relics in Minhe County (Figure 15). In addition, DEM (0.06263), topographic relief (0.03861), and NDVI (0.02697) also exhibit significant statistical correlations. These factors interact through various physical processes such as tectonic movements, human engineering activities, and climate change, collectively affecting surface stability.

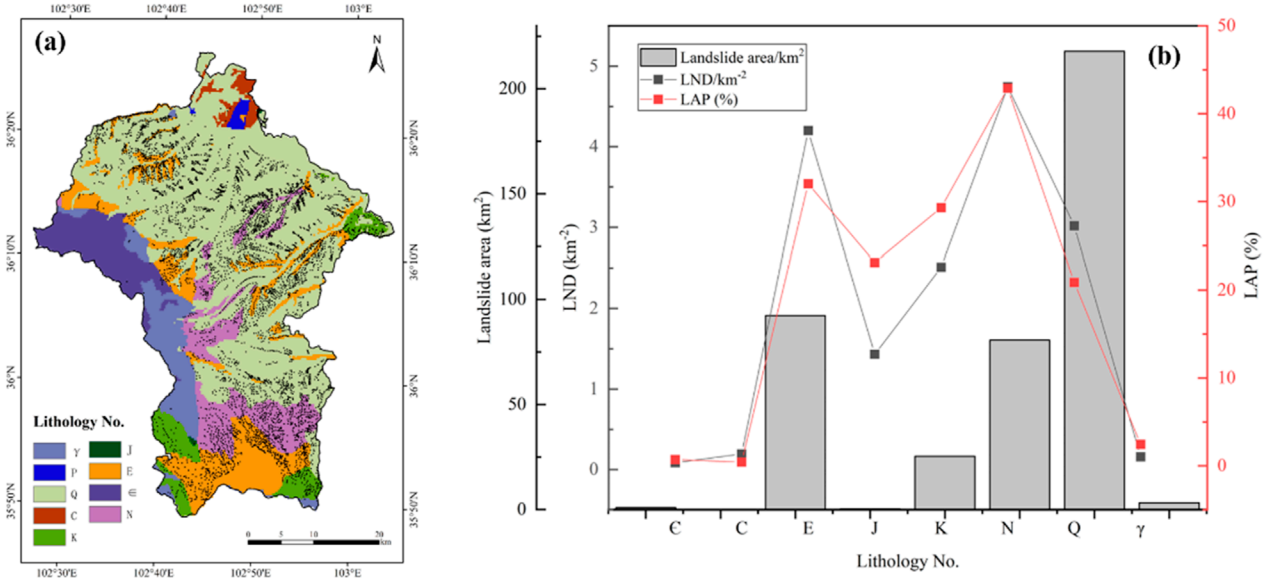

FIGURE 9
Relationship between lithology and landslide distribution. **(a)** Lithology distribution in the study area. **(b)** Statistics of landslide indicators in the lithology intervals. (Strata:Є-Cambrian,C-Carboniferous,E-Paleogene,J-Jurassic,K-Cretaceous,N-Neogene,O-Ordovician,P-Permian,Q-Quaternary,S-Silurian,γ-Intrusive rock).

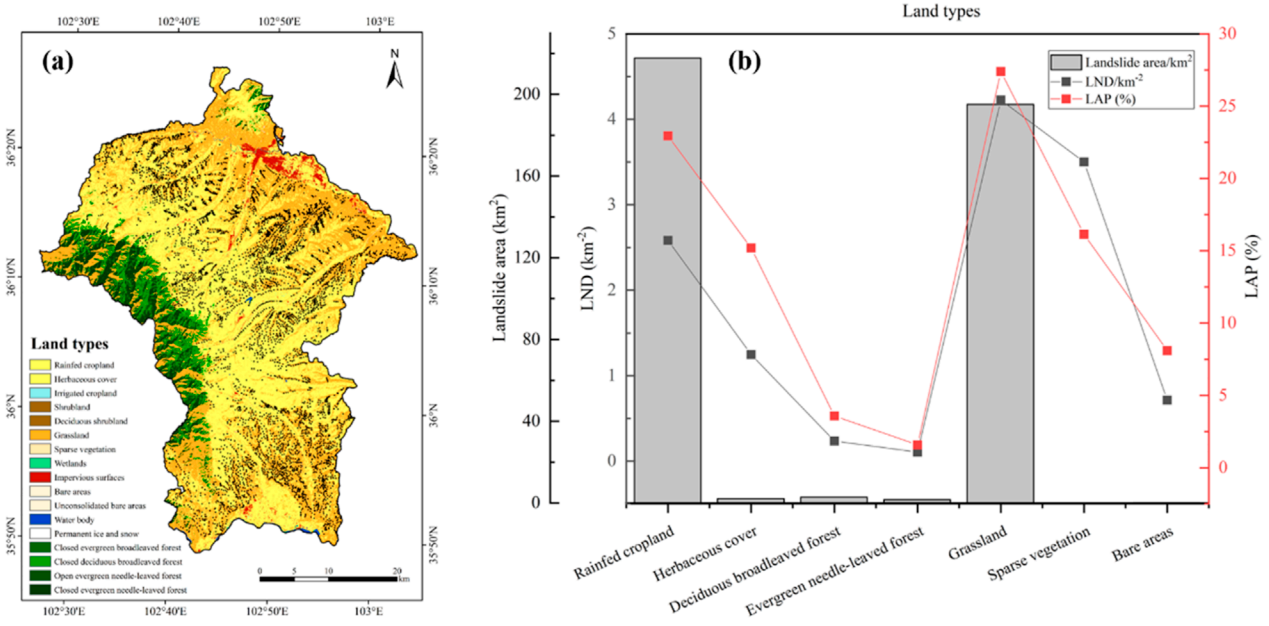

FIGURE 10
Relationship between land use type and landslide distribution. **(a)** Land use type distribution in the study area. **(b)** Statistics of landslide indicators in the land use type intervals.

Slope, as an important intrinsic condition for landslide occurrence (particularly shallow landslides), is one of the primary controlling factors for landslide development (Guo et al., 2013). Generally, the steeper the slope, the stronger the gravitational forces acting on the soil and rock masses, which reduces shear strength and makes landslides more likely (Mao et al., 2024). Aspect, on the other hand, influences the degree of solar radiation and precipitation received by a slope, further adjusting the degree of weathering and moisture content in the soil, thus significantly affecting slope stability. Additionally, aspect affects vegetation growth on the slope;

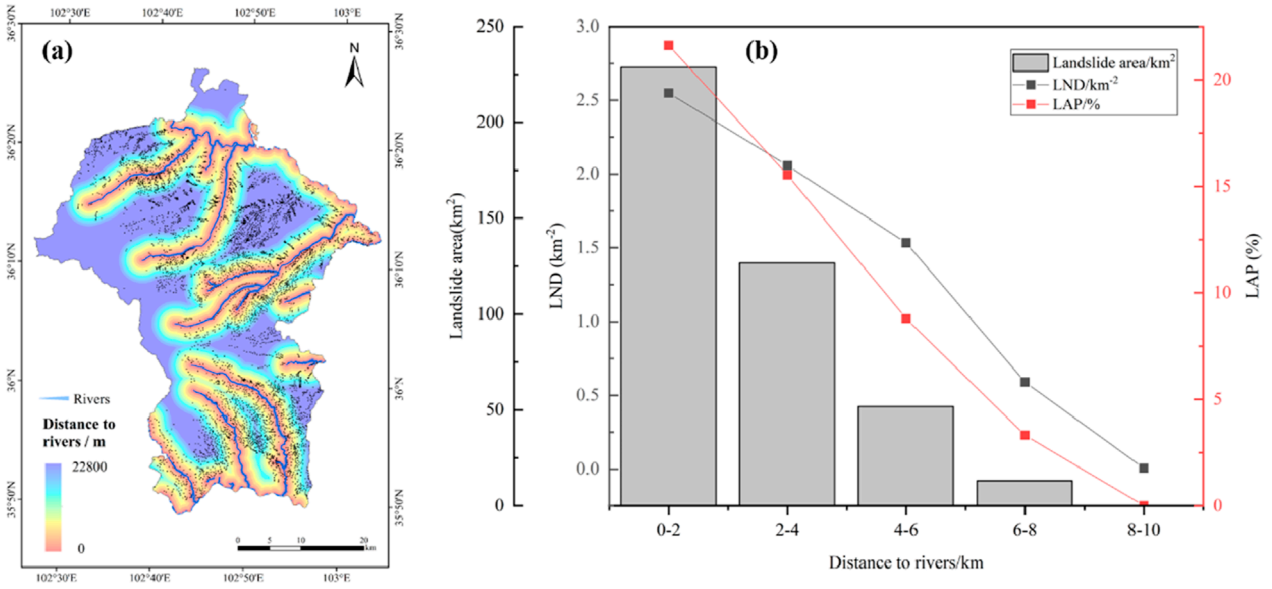

FIGURE 11
Relationship between the distance from rivers and the landslide distribution. **(a)** The distribution of the distance from rivers in the study area. **(b)** Statistics of landslide indicators in the intervals of the distance from rivers.

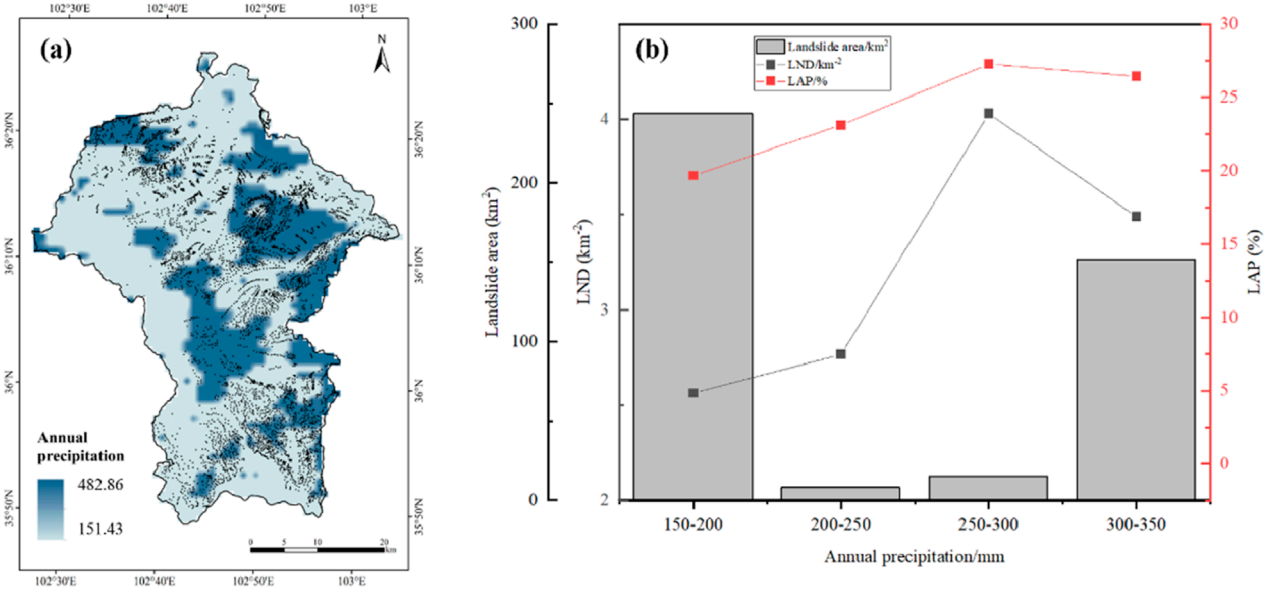

FIGURE 12
Relationship between average precipitation and landslide distribution. **(a)** Average precipitation distribution in the study area. **(b)** Statistics of landslide indicators in the average precipitation intervals.

sunny slopes typically have sparse vegetation and weaker erosion resistance, while shady slopes have denser vegetation but accumulate more moisture, potentially leading to shallow landslides.

In contrast, the influence of lithology (0.0048) and land use (0.0051) on the landslide relics in this region is relatively small. We hypothesize that the lower weight of lithology's impact may be related to several factors: first, the significant topographic relief in the study area makes the influence of gravity on slope stability more direct, overshadowing the effect of lithological differences on landslide formation. Second, the weathering degree of different lithological layers within the region may be relatively similar, which weakens the control of lithology on landslides. As for land use, its limited influence on landslides may be attributed to the fact that most of Minhe County is located in mountainous areas, where extensive natural vegetation is likely present, and land use changes are minimal. In such areas, vegetation plays a role in reinforcing slopes and conserving soil and water, thus reducing the direct impact of land use changes on landslide occurrence.

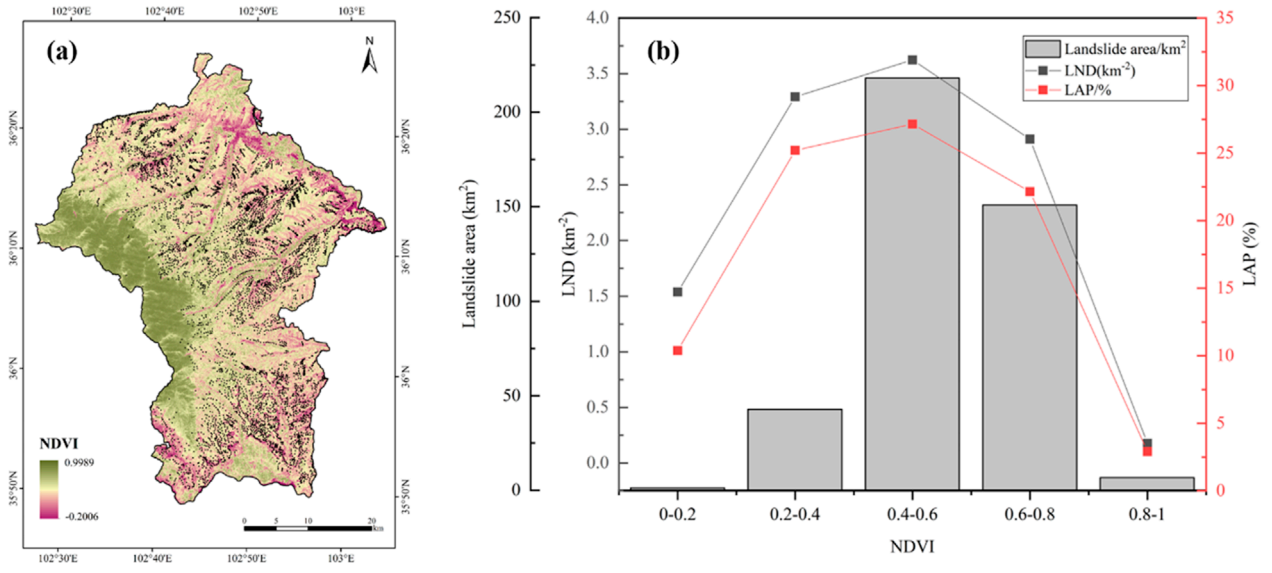

FIGURE 13
Relationship between NDVI and landslide distribution. **(a)** NDVI distribution in the study area. **(b)** Statistics of landslide indicators in the NDVI intervals.

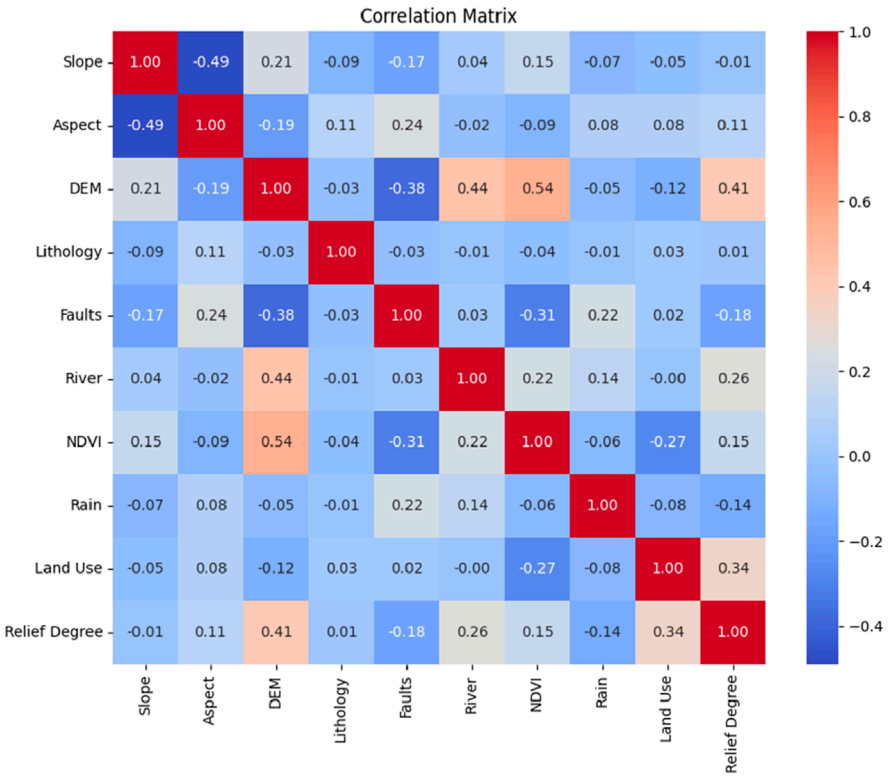

FIGURE 14
Pearson correlation coefficient analysis of influencing factors.

5 Discussion

5.1 Landslide inventory

A landslide inventory refers to the systematic organization of landslide characteristic information for a specific region, forming a database. The completeness of such an inventory is crucial to the accuracy of disaster assessments (Guo et al., 2024). Landslide inventories can be divided into event-based landslide inventories and historical landslide inventories. Event-based inventories record landslides triggered by a single event, such as earthquakes (Dai et al., 2011; Xu et al., 2014; Ma et al., 2024b; Shao et al., 2023a) or

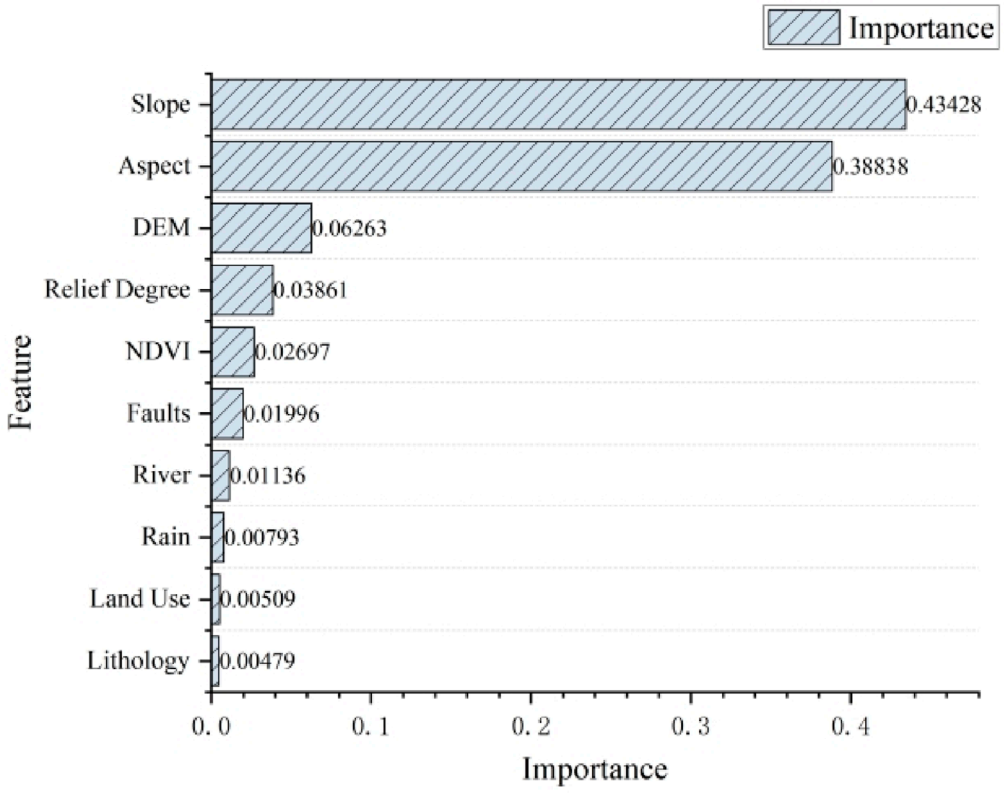

FIGURE 15
Importance of influencing factors.

rainfall (Ma et al., 2023c; Xie et al., 2023; Gao et al., 2024; Shao et al., 2023d). Historical landslide inventories, on the other hand, encompass landslide events accumulated over hundreds or even thousands of years (Chen J. et al., 2023; Li et al., 2022a; Li et al., 2022b; Shao et al., 2020). In our previous work, we focused on historical landslides and, using high-resolution satellite remote sensing imagery for interpretation, created the most comprehensive landslide relic inventory for Minhe County to date.

However, existing landslide surveys in Minhe County still need further refinement. Most current research in this region has focused on individual landslides (Mu et al., 2020), clustered landslides (Cui et al., 2008), or landslides triggered by single events. Only a few scholars have studied landslide distribution and disaster assessments in Minhe County. For instance, Kou et al. in their geological hazard investigation and zoning project, identified 224 landslide disasters in Minhe County (Kou et al., 2017). Zhao et al. used historical geological disaster data provided by the Qinghai Provincial Geological Environment Monitoring Station and found 569 landslide traces in Minhe (Zhao et al., 2021). Additionally, Peng et al. focused on the Loess Plateau region, conducting landslide interpretation and analysis of triggering mechanisms. They identified 14,544 landslides across the entire Loess Plateau, with 1,823 landslides located in the Haidong-Lanzhou-Tongwei area (HLTZ), covering a total area of 3,530 km^2 (Peng et al., 2019). Meng et al. using InSAR technology, created a comprehensive landslide inventory for the Huangshui River region, identifying 31 landslide traces in the 16,000 km^2 area (Meng et al., 2020). While these studies provided valuable references for our interpretation and cross-verification, the number of landslides identified in previous studies is far lower than the 5,517 landslide relics we identified.

Additionally, the southern Guanting Basin in Minhe County, located along the Longyangxia-Liujiaxia section of the upper Yellow River, is a region with frequent landslide disasters. In recent years, many scholars have studied the characteristics and mechanisms of landslides in this area. For example, Yin et al. identified 205 landslides of various sizes along this river section, with seven landslides located in the Guanting Basin, primarily mudstone landslides (Yin Z. et al., 2010). He et al. also obtained similar results (He et al., 2017). Among the landslide relics we identified, 260 are located in the Guanting Basin, far exceeding the number reported in existing studies.

In conclusion, the landslide inventory we developed in previous work is the most comprehensive and high-quality landslide database for Minhe County and its surrounding regions to date. Using this inventory, we analyzed the spatial distribution and possible controlling factors of landslides in Minhe, providing valuable insights. However, there are some limitations to our study. The method we used is based on human-assisted visual interpretation. For smaller landslides, due to the resolution limitations of satellite imagery or subjective interpretation, some landslides may have been missed. However, these omissions have a relatively small impact on

the overall accuracy of the inventory. In future research, we will consider integrating additional methods to address this limitation.

5.2 Spatial distribution of landslides

The areas with high point density and high area density of landslide relics in Minhe County generally exhibit similar spatial distributions, although some differences still exist. In the southwestern part of the county, the area density of landslides is more prominent compared to the point density, suggesting that the landslides in this region tend to be larger in scale. Conversely, in the northwestern part of the county, the point density of landslides is more significant.

The higher area density of landslides in the southwestern part of the county indicates that the region experiences more large-scale landslides. Our preliminary analysis suggests that the frequent occurrence of large-scale landslides in this area is the result of multiple geological, geomorphological, and environmental factors. The relatively steep slopes and topographic relief lead to the accumulation of gravitational potential energy, while fault structures cause rock fragmentation and weakening. The easily weathered Paleogene strata provide abundant landslide material, and river erosion continually undermines slope stability. Additionally, the abundant precipitation increases pore water pressure, and sparse vegetation exacerbates slope instability. These factors interact spatially, reinforcing one another, making large-scale, long-runout, and far-reaching landslides more likely to occur in this region.

In contrast, the more significant point density of landslides in the northwestern part of the county suggests a higher frequency of landslides, but the landslides are relatively smaller in scale. We believe this is mainly due to the relatively gentle slopes, stable geological structures, and widespread loose deposits in this region. While local topographic relief and rainfall conditions may trigger landslides, the lack of fault zones, weaker erosion at the slope toes, and limited thickness of loose materials contribute to the prevalence of shallow, small-scale landslides. Furthermore, the low vegetation coverage further reduces slope stability, increasing the frequency of landslides, though it does not significantly affect the scale of the landslides.

In addition, as noted by Kou et al. (2017), landslides in the study area show a certain degree of clustering, with high-risk landslide zones in Minhe County mainly distributed along the middle and lower reaches of the Huangshui River and the tributaries of the Yellow River. Our findings are consistent with this pattern. Wei et al. (2021) summarized the spatial distribution patterns of landslide hazards in Qinghai Province, taking into account administrative regions, geomorphology, agricultural and pastoral zones, and watershed divisions. Their study demonstrated that landslides are predominantly concentrated in the agricultural areas of the Huangshui River Basin in eastern Qinghai, further supporting our results.

Additionally, earthquakes, as a typical representation of neotectonic activity, can lead to a "sheet-like" dense distribution of landslides in loose soil (Li et al., 2021b), a phenomenon also reflected in our study. For example, following the 1987 earthquake in Xigou Township, Minhe County (magnitude 4.1), many landslides were densely distributed around the epicentral area (Figure 16). Active faults are potential sources of destructive earthquakes (Wu et al., 2024), and further research is needed to determine whether the landslides triggered by this earthquake are related to active faulting. We will continue to collect detailed geological data from the region to conduct an in-depth analysis of the mechanisms behind these earthquake-induced landslides.

5.3 Correlation between landslides and influencing factors

In terms of topographic factors, the majority of landslides in the study area occurred at elevations between 1,900 and 2,400 m, mostly in mid-high altitude, moderately rugged mountainous terrain, accounting for about 85.6% of the total. Other researchers have also found similar results (Li et al., 2021b; Qiu et al., 2018), where landslides are concentrated at elevations of 2,000–2,800 m. This range corresponds to mid-low mountain hilly areas, adjacent to river valley alluvial plains. We believe that the dense distribution of landslides in this elevation range is closely related to the well-developed erosion gullies in the area. Additionally, the intensity of human activity in this elevation range plays a significant role in landslide development (Tian et al., 2024; Zhang et al., 2015; Zhao et al., 2021).

Slope gradient is another crucial factor influencing slope stability (Ma et al., 2023b). Our results show that most landslides occurred on slopes with gradients between 10° and 40°, mainly concentrated in the 15°–20° range. This is consistent with previous studies. For example, Li et al. (2024b) found that in the upper reaches of the Yellow River, including the Guanting Basin in Minhe County, landslides are primarily concentrated on slopes between 15° and 40°, with most in the 15°–20° and 35°–40° ranges. Field surveys also revealed that most landslides in the 15°–20° range are relatively stable, with a low likelihood of further movement. However, those in the 35°–40° range are more unstable and may reactivate under heavy or prolonged rainfall. Wang et al. (2015) reached similar conclusions, noting that slopes with a gradient of 15°–30° contribute the most to landslide development, followed by slopes of 10°–15° and 30°–40°, while slopes less than 10° and greater than 40° contribute the least. However, Zhou et al. (2013) presented a different view, suggesting that geological disasters in the Huangshui River Basin, particularly in loess regions, occur mainly on steep slopes of 30°–60°. Variations in slope gradients across different studies are common in landslide research. We believe that, aside from the southwestern mountainous area, the overall terrain in Minhe County is relatively flat, leading to lower overall slope gradients in landslide-affected areas. Furthermore, landslide relics often represent older events, and over time, unstable landslides may move or shift, resulting in a gradual decrease in slope gradients.

The properties of the soil and rock also affect slope stability. In terms of lithostratigraphy, the study area is primarily composed of Quaternary deposits, Paleogene strata, and Neogene strata. Among these, Quaternary deposits have the largest exposed area, covering 54.77% of the total study area and predominantly distributed across the northern, central, and eastern regions of Minhe County. The Paleogene and Neogene formations follow, accounting for 15.13% and 9.87% of the study area, respectively. The occurrence of landslides is closely associated with lithological

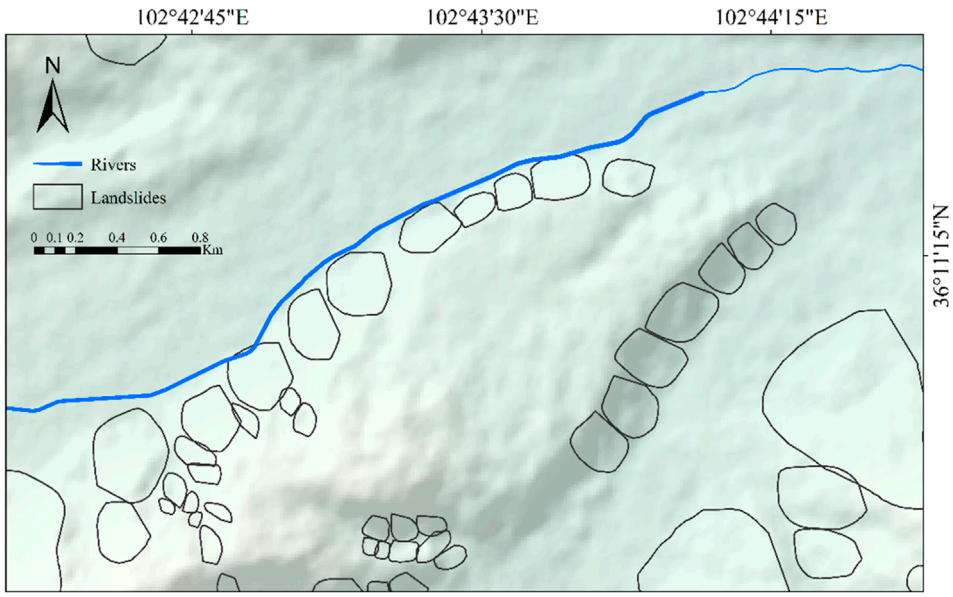

FIGURE 16
Distribution of landslides in the vicinity of the earthquake.

characteristics. Studies have demonstrated that landslides are most prevalent in Quaternary loess deposits, with a total of 3,150 recorded landslides in these formations, a trend consistent with the findings of Li et al. (2021a). Additionally, the primary lithological components of regional slopes include Late Pleistocene loess and Neogene mudstone, both of which significantly influence slope stability due to their unique geotechnical properties. Neogene mudstone is characterized by a high clay mineral content (Xin et al., 2017), making it highly susceptible to softening upon water infiltration. This hydration-induced weakening substantially reduces shear strength, facilitating the formation of sliding zones and increasing the likelihood of slope failure. Similarly, Quaternary loess exhibits large porosity, well-developed vertical joints, and high permeability. These attributes render it particularly prone to softening and slope instability when subjected to prolonged rainfall infiltration (Huang et al., 2022). Collectively, these lithological and hydrogeological characteristics create favorable conditions for landslide initiation and evolution in the region. A deeper understanding of the influence of different lithological units on slope stability is essential for improving landslide susceptibility assessment and providing a scientific foundation for regional geohazard prevention and mitigation strategies.

Land use in Minhe County is predominantly grassland, cropland, and forest. Landslides mainly occur in grassland and cropland areas, likely influenced by human activities and agricultural irrigation (Huang et al., 2022). Agriculture is the main livelihood in the loess regions, and long-term irrigation raises the groundwater level, leading to soil deformation at the base of slopes and slope instability. The frequent landslides in the Heifangtai region of Gansu are a typical example of this (Xu and Yan, 2019).

The Huangshui River is the most important tributary of the upper Yellow River, and its river channel is highly meandering in the study area. In this phase, intense river erosion leads to stress transfer in the valleys, causing slope unloading and fracturing, which increases the instability of rock masses (Zhao et al., 2021). Our results show that most landslides occur within 0–2 km from the river, and both the number and area of landslides decrease as the distance from the river increases. This indicates that river erosion is one of the main factors influencing landslides in the region.

The NDVI reflects the extent of vegetation cover, with higher NDVI values representing denser vegetation. Landslides in the study area are primarily concentrated in areas with NDVI values between 0.4 and 0.8. This result differs from the commonly held view that landslides are more likely to occur in areas with sparse vegetation (Chen et al., 2021). Minhe County is mostly composed of mid-low mountain hilly areas, except for its western highlands. We speculate that most of the area has relatively good vegetation cover, but the root systems are shallow, primarily concentrated in the topsoil layer. The significant difference in soil properties between the root layer and the subsoil makes it easy to trigger large-scale shallow landslides, especially during short periods of heavy rainfall (Xu et al., 2022). Huang Hengwei (Huang, 2017) also supports a similar viewpoint. Additionally, with the implementation of the "Green is Gold" ecological protection policy, vegetation cover in Minhe County has been increasing, which may have affected the NDVI values used in this study, potentially introducing some statistical bias.

In our analysis of fault-related factors, we found no significant correlation between landslide distribution and distance from faults. If we only consider the number and area of landslides, we observe that both decrease as the distance from faults increases. However, this does not necessarily suggest an objective or reliable conclusion. Our analysis shows that LND and LAP peak at a distance of 12–15 km from faults, while the values are lowest at 0–3 km. This suggests that the influence of faults is limited and that landslide causality in the region is highly complex. Further research will be required to explore this in more detail.

5.4 Policy recommendations and future research directions

Based on the spatial distribution characteristics of landslides, the study found that landslide relics in Minhe County are primarily distributed in areas with an elevation of 2,000–2,100 m, slopes of 15°–25°, aspects facing west or northwest, Quaternary strata, and within 0–2 km from rivers. Given these spatial characteristics, future disaster prevention and mitigation efforts should prioritize monitoring and management of areas near riverbanks and those with vulnerable lithology. The government and relevant departments can use these spatial data to scientifically plan monitoring areas, especially in regions with critical infrastructure and high population density, to effectively reduce the potential risks of landslide disasters (Nanehkaran et al., 2023). Moreover, these spatial data provide a solid foundation for subsequent risk prediction and emergency management, enabling rapid identification of high-risk areas and the scientific allocation of disaster prevention resources.

In the quantitative analysis of the overall spatial distribution of landslides, the LND and LAP indices clarified the spatial distribution density of landslides in Minhe County, providing a more precise basis for landslide disaster risk assessment. Through the analysis of these quantitative indicators, the study found that the landslide area density is more significant in the southwestern region, while the landslide point density is higher in the northwestern region. This suggests that, in subsequent geological disaster risk prevention and control efforts, special attention should be given to the larger-scale landslides in the southwestern region, while strengthening the monitoring and prevention of shallow and medium-sized landslides in the northwestern region. Based on these regional risk characteristics, differentiated landslide monitoring and management strategies should be implemented. In areas with high landslide point density, it is essential to strengthen emergency response mechanisms and develop detailed contingency plans to ensure rapid and effective emergency response during disaster events, thereby reducing the harm caused by landslides and protecting public safety.

From the perspective of key influencing factors, slope and aspect are the most important factors affecting landslide occurrence in Minhe County. The study indicates that landslides are frequent in areas with a slope of 15°–25° and a westward or northwestward aspect. Therefore, disaster prevention and mitigation strategies should prioritize addressing these key topographic factors. For example, in areas with steeper slopes, measures such as slope reinforcement and vegetation restoration should be implemented to enhance slope stability. In regions with significant aspects, monitoring of precipitation and water flow should be strengthened to reduce water-induced erosion and prevent slope instability. Additionally, landslide occurrences are typically the result of the interaction of multiple factors (Nikoobakht et al., 2022). For other factors that show significant statistical correlations (e.g., elevation, topographic relief, NDVI), comprehensive mitigation measures should be adopted based on specific regional conditions, such as improving slope drainage systems, reinforcing slope structures, and restoring vegetation, to effectively reduce the risk of landslides.

Overall, the findings of this study not only contribute to a deeper understanding of the triggering factors and distribution patterns of landslide relics in Minhe County, but also provide a scientific basis for subsequent landslide evaluation, early warning, and disaster prevention efforts. Moreover, the analytical methods used in this study are not only applicable to Minhe County but also have strong generalizability. These methods can be widely applied to other regions with similar geological and environmental conditions, providing effective support for landslide disaster risk assessment, monitoring and early warning, and emergency response. Similar research methods have already been successfully applied in several landslide-prone areas, providing valuable insights for disaster prevention in these regions. In future work, we will integrate field investigation data to validate and deepen our findings. We will optimize evaluation models, conduct landslide susceptibility assessments, and comprehensively consider the impact of multiple environmental factors and potential additional influences, thereby achieving a more comprehensive understanding of landslide causality. This will provide a more scientific basis for the prediction and management of geological disasters in Minhe County.

6 Conclusion

Based on the GIS platform, this study conducted an in-depth exploration of the spatial distribution and triggering factors of landslides, using the previously constructed landslide relic inventory of Minhe County, Qinghai Province, China. The earlier work identified 5,517 landslide features in Minhe County, with a total coverage area of 434.43 km^2, accounting for approximately 22.98% of the county's total area. Using landslide number density (LND) and landslide area percentage (LAP) as evaluation indicators, we performed a statistical analysis of the correlation between landslides and influencing factors. The results indicate that the LND and LAP indices for Minhe County are 13.17 km^{-2} and 87.38%, respectively. Furthermore, landslide relics are mainly distributed in the elevation range of 2,000–2,100 m, where the number of landslides and the landslide area account for 20.35% and 39.23% of the total, respectively. The 15°–25° slope gradient range is the most favorable for landslide development in the study area. Due to factors such as solar radiation and soil conditions, landslides are more likely to occur on west and northwest-facing slopes. Relief degree of land surface values between 150 and 200 are favorable for landslide development, and the 12–15 km range from fault lines is where LAP and LND peak, at 4.88 km^{-2} and 6.29%, respectively. Neogene strata are the main geological formations promoting landslide development. Compared to other land types, grasslands exhibit a higher probability of landslide occurrence. LND and LAP values decrease as the distance from rivers increases, with the 0–2 km range being more prone to landslides. The 250–300 mm annual rainfall range is the most favorable for landslide development, while areas with NDVI values of 0.4–0.6 are more susceptible to landslides. Slope and aspect are the most significant factors influencing the landslide relics in Minhe County, while the influence of lithology and land use is relatively low. The results of this study contribute to a better understanding of the triggering factors and spatial distribution patterns of landslide relics in the region, providing crucial support for future landslide risk assessments and local disaster prevention and mitigation efforts.

Data availability statement

The datasets used and/or analyzed during the current study are available from the corresponding author on reasonable request.

Author contributions

QW: Conceptualization, Data curation, Formal Analysis, Investigation, Methodology, Validation, Visualization, Writing–original draft, Writing–review and editing. CX: Conceptualization, Funding acquisition, Resources, Software, Supervision, Writing–review and editing.

Funding

The author(s) declare that financial support was received for the research and/or publication of this article. This research was funded by the National Institute of Natural Hazards, Ministry of Emergency Management of China (2023-JBKY-57) and the National Natural Science Foundation of China (42077259).

Acknowledgments

We would like to express my sincere gratitude to the reviewers for their professional advice and valuable feedback. Their review not only helped to make the content of this paper more accurate and rigorous but also provided important guidance for its quality improvement. I sincerely appreciate their time and effort devoted to the enhancement of this paper.

Conflict of interest

The authors declare that the research was conducted in the absence of any commercial or financial relationships that could be construed as a potential conflict of interest.

The author(s) declared that they were an editorial board member of Frontiers, at the time of submission. This had no impact on the peer review process and the final decision.

Publisher's note

All claims expressed in this article are solely those of the authors and do not necessarily represent those of their affiliated organizations, or those of the publisher, the editors and the reviewers. Any product that may be evaluated in this article, or claim that may be made by its manufacturer, is not guaranteed or endorsed by the publisher.

Supplementary material

The Supplementary Material for this article can be found online at: https://www.frontiersin.org/articles/10.3389/feart.2025.1501498/full#supplementary-material

References

Ali, S. A., Parvin, F., Vojteková, J., Costache, R., Linh, N. T. T., Pham, Q. B., et al. (2021). GIS-based landslide susceptibility modeling: a comparison between fuzzy multi-criteria and machine learning algorithms. *Geosci. Front.* 12, 857–876. doi:10.1016/j.gsf.2020.09.004

Breiman, L. (2001). Random forests. *Mach. Learn.* 45, 5–32. doi:10.1023/a:1010933404324

Bui, D. T., Pradhan, B., Lofman, O., Revhaug, I., and Dick, O. B. (2012). Landslide susceptibility mapping at Hoa Binh Province (Vietnam) using an adaptive neuro-fuzzy inference system and GIS. *Comput. and Geosciences* 45, 199–211. doi:10.1016/j.cageo.2011.10.031

Cemiloglu, A., Zhu, L., Mohammednour, A. B., Azarafza, M., and Nanehkaran, Y. A. (2023). Landslide susceptibility assessment for Maragheh County, Iran, using the logistic regression algorithm. *Land* 12, 1397. doi:10.3390/land12071397

Chen, B., Li, Z., Zhang, C., Ding, M., Zhu, W., Zhang, S., et al. (2022). Wide area detection and distribution characteristics of landslides along Sichuan expressways. *Remote Sens.* 14, 3431. doi:10.3390/rs14143431

Chen, J., Li, L., Xu, C., Huang, Y., Luo, Z., Xu, X., et al. (2023a). Freely accessible inventory and spatial distribution of large-scale landslides in Xianyang City, Shaanxi Province, China. *Earthq. Res. Adv.* 3, 100217. doi:10.1016/j.eqrea.2023.100217

Chen, L., Ma, P., Yu, C., Zheng, Y., Zhu, Q., and Ding, Y. (2023b). Landslide susceptibility assessment in multiple urban slope settings with a landslide inventory augmented by InSAR techniques. *Eng. Geol.* 327, 107342. doi:10.1016/j.enggeo.2023.107342

Chen, W., Chen, X., Peng, J., Panahi, M., and Lee, S. (2021). Landslide susceptibility modeling based on ANFIS with teaching-learning-based optimization and Satin bowerbird optimizer. *Geosci. Front.* 12, 93–107. doi:10.1016/j.gsf.2020.07.012

Chen, Z., Huang, Y., He, X., Shao, X., Li, L., Xu, C., et al. (2023c). Landslides triggered by the 10 June 2022 Maerkang earthquake swarm, Sichuan, China: spatial distribution and tectonic significance. *Landslides* 20, 2155–2169. doi:10.1007/s10346-023-02080-0

Chowdhury, M. S., Rahman, M. N., Sheikh, M. S., Sayeid, M. A., Mahmud, K. H., and Hafsa, B. (2024). GIS-based landslide susceptibility mapping using logistic regression, random forest and decision and regression tree models in Chattogram District, Bangladesh. *Heliyon* 10, e23424. doi:10.1016/j.heliyon.2023.e23424

Cui, F., Hu, R., Tan, R., Yang, K., Yu, J., Zhang, M., et al. (2008). Study on formation mechanism and stability evaluation of Badashan landslide group in Qinghai province. *Chin. J. Rock Mech. Eng.* 27, 848–857. (in Chinese)

Cui, F., Xiong, C., Wu, Q., Xu, C., Li, N., Wu, N., et al. (2021). Dynamic response of the Daguangbao landslide triggered by the Wenchuan earthquake with a composite hypocenter. *Geomatics, Nat. Hazards Risk* 12, 2170–2193. doi:10.1080/19475705.2021.1944916

Cui, P., Su, F., Zou, Q., Chen, N., and Zhang, Y. (2015). Risk assessment and disaster reduction strategies for mountainous and meteorological hazards in Tibetan Plateau. *Chin. Sci. Bull.* 60, 3067–3077. doi:10.1360/n972015-00849

Cui, Y., Hu, J., Zheng, J., Fu, G., and Xu, C. (2022). Susceptibility assessment of landslides caused by snowmelt in a typical loess area in the Yining County, Xinjiang, China. *Q. J. Eng. Geol. Hydrogeology* 55, qjegh2021–2024. doi:10.1144/qjegh2021-024

Cui, Y., Yang, L., Xu, C., and Zheng, J. (2024). Spatial distribution of shallow landslides caused by typhoon lekima in 2019 in zhejiang province, China. *J. Mt. Sci.* 21, 1564–1580. doi:10.1007/s11629-023-8377-y

Cutler, A., Cutler, D. R., and Stevens, J. R. (2012). *Random forests*. Ensemble Machine Learning: Methods and Applications, New York, NY: Springer 157–175.

Dai, F. C., Xu, C., Yao, X., Xu, L., Tu, X. B., and Gong, Q. M. (2011). Spatial distribution of landslides triggered by the 2008 Ms 8.0 Wenchuan earthquake, China. *J. Asian Earth Sci.* 40, 883–895. doi:10.1016/j.jseaes.2010.04.010

Du, J., Glade, T., Woldai, T., Chai, B., and Zeng, B. (2020). Landslide susceptibility assessment based on an incomplete landslide inventory in the Jilong Valley, Tibet, Chinese Himalayas. *Eng. Geol.* 270, 105572. doi:10.1016/j.enggeo.2020.105572

Feng, L., Xu, C., Tian, Y., Li, L., Sun, J., Huang, Y., et al. (2024). Landslides of China's qinling. *Geoscience Data J.* doi:10.1002/gdj3.246

Frattini, P., and Crosta, G. B. (2013). The role of material properties and landscape morphology on landslide size distributions. *Earth Planet. Sci. Lett.* 361, 310–319. doi:10.1016/j.epsl.2012.10.029

Froude, M. J., and Petley, D. N. (2018). Global fatal landslide occurrence from 2004 to 2016. *Nat. Hazards Earth Syst. Sci.* 18, 2161–2181. doi:10.5194/nhess-18-2161-2018

Gao, H., Xu, C., Xie, C., Ma, J., and Xiao, Z. (2024). Landslides triggered by the july 2023 extreme rainstorm in the haihe River Basin, China. *Landslides* 21, 2885–2890. doi:10.1007/s10346-024-02322-9

Guo, F., Lai, P., Huang, F., Liu, L., Wang, X., and He, Z. (2024). Literature review and research progress of landslide susceptibility mapping based on knowledge graph. *Earth Sci.* 49, 1584–1606. doi:10.3799/dqkx.2023.058

Guo, G., Chen, Y., Li, M., and Dang, J. (2013). Statistic relationship between slope gradient and landslide probability in soil slopes around reservoir. *J. Eng. Geol.* 21, 0607. (in Chinese). doi:10.3969/j.issn.1004-9665.2013.04.018

Guzzetti, F., Mondini, A. C., Cardinali, M., Fiorucci, F., Santangelo, M., and Chang, K.-T. (2012). Landslide inventory maps: new tools for an old problem. *Earth-Science Rev.* 112, 42–66. doi:10.1016/j.earscirev.2012.02.001

He, Y., Zhang, D., Li, Y., Han, Y., and Xue, B. (2017). The study of landslide characteristics in the mainstream area of the upper Yellow River based on clustering. *Geospatial Inf.* 15, 5. (in Chinese). doi:10.3969/j.issn.1672-4623.2017.11.019

Hong, H., Liu, J., and Zhu, A. X. (2020). Modeling landslide susceptibility using LogitBoost alternating decision trees and forest by penalizing attributes with the bagging ensemble. *Sci. Total Environ.* 718, 137231. doi:10.1016/j.scitotenv.2020.137231

Huang, H. (2017). *The research of relationship between "9.16" mass of shallow landslide in Changning, Yunnan and vegetation type*. Kunming, China: Kunming University of Science and Technology.

Huang, Y., Xu, C., Li, L., He, X., Cheng, J., Xu, X., et al. (2022). Inventory and spatial distribution of ancient landslides in Hualong County, China. *Land* 12, 136. doi:10.3390/land12010136

Huang, Y., Xu, C., Zhang, X., Li, L., and Xu, X. (2023). Research in the field of natural hazards based on bibliometric analysis. *Nat. Hazards Rev.* 24, 04023012. doi:10.1061/nhrefo.nheng-1739

Korup, O. (2005). Distribution of landslides in southwest New Zealand. *Landslides* 2, 43–51. doi:10.1007/s10346-004-0042-0

Kou, L., Bian, J., Zhang, T., Zhao, W., and Wang, H. (2017). The application of GIS-based information method in susceptibility evaluation of regional geological hazards in Minhe County, Qinghai Province. *Northwest. Geol.* 50, 244–248. (in Chinese). doi:10.3969/j.issn.1009-6248.2017.02.025

Kubwimana, D., Ait Brahim, L., Nkurunziza, P., Dille, A., Depicker, A., Nahimana, L., et al. (2021). Characteristics and distribution of landslides in the populated hillslopes of Bujumbura, Burundi. *Geosciences* 11, 259. doi:10.3390/geosciences11060259

Li, L., Xu, C., Xu, X., Zhang, Z., and Cheng, J. (2021a). Inventory and distribution characteristics of large-scale landslides in Baoji city, Shaanxi province, China. *ISPRS Int. J. Geo-Information* 11, 10. doi:10.3390/ijgi11010010

Li, L., Xu, C., Yang, Z., Zhang, Z., and Lv, M. (2022a). An inventory of large-scale landslides in Baoji city, Shaanxi province, China. *Data* 7, 114. doi:10.3390/data7080114

Li, L., Xu, C., Yao, X., Shao, B., Ouyang, J., Zhang, Z., et al. (2022b). Large-scale landslides around the reservoir area of Baihetan hydropower station in Southwest China: analysis of the spatial distribution. *Nat. Hazards Res.* 2, 218–229. doi:10.1016/j.nhres.2022.07.002

Li, L., Xu, C., Zhang, Z., and Huang, Y. (2021b). Spatial distribution and its control factors of landslides in longxi county, Gansu province, China. *IOP Conf. Ser. Earth Environ. Sci.* 861, 052013. doi:10.1088/1755-1315/861/5/052013

Li, T., Xie, C., Xu, C., Qi, W., Huang, Y., and Li, L. (2024a). Automated machine learning for rainfall-induced landslide hazard mapping in Luhe County of Guangdong Province, China China Geology, 7, 315–329. doi:10.31035/cg2024064

Li, Z., Wei, S., Wu, K., Sha, Y., Zhang, X., Li, D., et al. (2024b). Study on temporal and spatial distribution of landslides in the upper reaches of the Yellow River. *Appl. Sci.* 14, 5488. doi:10.3390/app14135488

Lin, W., Chou, W., and Lin, C. (2008). Earthquake-induced landslide hazard and vegetation recovery assessment using remotely sensed data and a neural network-based classifier: a case study in central Taiwan. *Nat. Hazards* 47, 331–347. doi:10.1007/s11069-008-9222-x

Liu, R., Yang, X., Xu, C., Wei, L., and Zeng, X. (2022). Comparative study of convolutional neural network and conventional machine learning methods for landslide susceptibility mapping. *Remote Sens.* 14, 321. doi:10.3390/rs14020321

Ma, S., Chen, J., and Wu, S. e. (2024a). Distribution characteristics and susceptibility assessment of landslide hazards in Yinghu Town, Ankang, Shaanxi. *Geosciences* 38, 437–450. (in Chinese). doi:10.19657/j.geoscience.1000-8527.2023.067

Ma, S., Shao, X., Li, K., and Xu, C. (2024b). Landslides triggered by the 30th june 2012 Ms6. 6 hejing earthquake, xinjiang province, China. *Bull. Eng. Geol. Environ.* 83, 256. doi:10.1007/s10064-024-03727-5

Ma, S., Shao, X., and Xu, C. (2022). Characterizing the distribution pattern and a physically based susceptibility assessment of shallow landslides triggered by the 2019 heavy rainfall event in Longchuan County, Guangdong Province, China. *Remote Sens.* 14, 4257. doi:10.3390/rs14174257

Ma, S., Shao, X., and Xu, C. (2023a). Estimating the quality of the most popular machine learning algorithms for landslide susceptibility mapping in 2018 Mw 7.5 Palu earthquake. *Remote Sens.* 15, 4733. doi:10.3390/rs15194733

Ma, S., Shao, X., and Xu, C. (2023b). Landslide susceptibility mapping in terms of the slope-unit or raster-unit, which is better? *J. Earth Sci.* 34, 386–397. doi:10.1007/s12583-021-1407-1

Ma, S., Shao, X., and Xu, C. (2023c). Landslides triggered by the 2016 heavy rainfall event in Sanming, Fujian Province: distribution pattern analysis and spatio-temporal susceptibility assessment. *Remote Sens.* 15, 2738. doi:10.3390/rs15112738

Ma, S., Shao, X., and Xu, C. (2023d). Physically-based rainfall-induced landslide thresholds for the Tianshui area of Loess Plateau, China by TRIGRS model. *Catena* 233, 107499. doi:10.1016/j.catena.2023.107499

Ma, S., Shao, X., and Xu, C. (2024c). Delineating Non-Susceptible landslide areas in China based on topographic index and quantile Non-Linear model. *Forests* 15, 678. doi:10.3390/f15040678

Ma, S., Shao, X., and Xu, C. (2024d). Potential controlling factors and landslide susceptibility features of the 2022 Ms 6.8 Luding Earthquake. *Remote Sens.* 16, 2861. doi:10.3390/rs16152861

Mao, Y., Li, Y., Teng, F., Sabonchi, A. K., Azarafza, M., and Zhang, M. (2024). Utilizing hybrid machine learning and soft computing techniques for landslide susceptibility mapping in a Drainage Basin. *Water* 16, 380. doi:10.3390/w16030380

Meng, Q., Confuorto, P., Peng, Y., Raspini, F., Bianchini, S., Han, S., et al. (2020). Regional recognition and classification of active loess landslides using two-dimensional deformation derived from Sentinel-1 interferometric radar data. *Remote Sens.* 12, 1541. doi:10.3390/rs12101541

Mu, W., Wu, X., Qian, C., and Wang, K. (2020). Triggering mechanism and reactivation probability of loess-mudstone landslides induced by rainfall infiltration: a case study in Qinghai Province, Northwestern China. *Environ. Earth Sci.* 79, 22. doi:10.1007/s12665-019-8767-1

Nanehkaran, Y. A., Chen, B., Cemiloglu, A., Chen, J., Anwar, S., Azarafza, M., et al. (2023). Riverside landslide susceptibility overview: leveraging artificial neural networks and machine learning in accordance with the United Nations (UN) sustainable development goals. *Water* 15, 2707. doi:10.3390/w15152707

Nanehkaran, Y. A., Licai, Z., Chen, J., Azarafza, M., and Yimin, M. (2022). Application of artificial neural networks and geographic information system to provide hazard susceptibility maps for rockfall failures. *Environ. Earth Sci.* 81, 475. doi:10.1007/s12665-022-10603-6

Naseer, S., Haq, T. U., Khan, A., Tanoli, J. I., Khan, N. G., Qaiser, F.-u.-R., et al. (2021). GIS-based spatial landslide distribution analysis of district Neelum, AJ&K, Pakistan. *Nat. Hazards* 106, 965–989. doi:10.1007/s11069-021-04502-5

Nikoobakht, S., Azarafza, M., Akgün, H., and Derakhshani, R. (2022). Landslide susceptibility assessment by using convolutional neural network. *Appl. Sci.* 12, 5992. doi:10.3390/app12125992

Peng, J., Wang, S., Wang, Q., Zhuang, J., Huang, W., Zhu, X., et al. (2019). Distribution and genetic types of loess landslides in China. *J. Asian Earth Sci.* 170, 329–350. doi:10.1016/j.jseaes.2018.11.015

Petley, D. (2012). Global patterns of loss of life from landslides. *Geology* 40, 927–930. doi:10.1130/g33217.1

Piacentini, D., Troiani, F., Daniele, G., and Pizziolo, M. (2018). Historical geospatial database for landslide analysis: the catalogue of landslide OCcurrences in the emilia-romagna region (CLOCkER). *Landslides* 15, 811–822. doi:10.1007/s10346-018-0962-8

Qin, Y., Yang, G., Lu, K., Sun, Q., Xie, J., and Wu, Y. (2021). Performance evaluation of five GIS-Based models for landslide susceptibility prediction and mapping: a case study of Kaiyang County, China. *Sustainability* 13, 6441. doi:10.3390/su13116441

Qiu, H., Cui, P., Regmi, A. D., Hu, S., Zhang, Y., and He, Y. (2018). Landslide distribution and size versus relative relief (Shaanxi Province, China). *Bull. Eng. Geol. Environ.* 77, 1331–1342. doi:10.1007/s10064-017-1121-5

Quan, H., Moon, H., Jin, G., and Park, S. (2014). Landslide susceptibility analysis in Baekdu Mountain Area using ANN and AHP method. *J. Korean Geo-Environmental Soc.* 15, 79–85. doi:10.14481/jkges.2014.15.12.79

Selamat, S. N., Majid, N. A., and Taha, M. R. (2024). Multicollinearity and spatial correlation analysis of landslide conditioning factors in Langat River Basin, Selangor. *Nat. Hazards* 121, 2665–2684. doi:10.1007/s11069-024-06903-8

Shao, X., Ma, S., and Xu, C. (2023a). Distribution and characteristics of shallow landslides triggered by the 2018 Mw 7.5 Palu earthquake, Indonesia. *Landslides* 20, 157–175. doi:10.1007/s10346-022-01972-x

Shao, X., Ma, S., and Xu, C. (2023b). Hazard assessment modeling and software development of earthquake-triggered landslides in the Sichuan–Yunnan area, China. *Geosci. Model Dev.* 16, 5113–5129. doi:10.5194/gmd-16-5113-2023

Shao, X., Ma, S., Xu, C., Cheng, J., and Xu, X. (2023c). Seismically-induced landslide probabilistic hazard mapping of Aba Prefecture and Chengdu Plain region, Sichuan Province, China for future seismic scenarios. *Geosci. Lett.* 10, 55. doi:10.1186/s40562-023-00307-5

Shao, X., Ma, S., Xu, C., Shen, L., and Lu, Y. (2020). Inventory, distribution and geometric characteristics of landslides in baoshan city, yunnan province, China. *Sustainability* 12, 2433. doi:10.3390/su12062433

Shao, X., Ma, S., Xu, C., Xie, C., Li, T., Huang, Y., et al. (2024a). Landslides triggered by the 2022 Ms. 6.8 Luding strike-slip earthquake: an update. *Eng. Geol.* 335, 107536. doi:10.1016/j.enggeo.2024.107536

Shao, X., Ma, S., Xu, C., and Xu, Y. (2023d). Insight into the characteristics and triggers of loess landslides during the 2013 heavy rainfall event in the Tianshui Area, China. *Remote Sens.* 15, 4304. doi:10.3390/rs15174304

Shao, X., Xu, C., Li, L., Yang, Z., Yao, X., Shao, B., et al. (2024b). Spatial analysis and hazard assessment of Large-scale ancient landslides around the reservoir area of Wudongde Hydropower Station, China. *Nat. Hazards* 120, 87–105. doi:10.1007/s11069-023-06201-9

Shao, X., Xu, C., and Ma, S. (2022). Preliminary analysis of coseismic landslides induced by the 1 June 2022 Ms 6.1 Lushan Earthquake, China. *Sustainability* 14, 16554. doi:10.3390/su142416554

Sun, J., Xu, C., Feng, L., Li, L., Zhang, X., and Yang, W. (2024). The Yinshan Mountains record over 10,000 landslides. *Data* 9, 31. doi:10.3390/data9020031

Tian, N., Lan, H., Li, L., Peng, J., Fu, B., and Clague, J. J. (2024). Human activities are intensifying the spatial variation of landslides in the Yellow River Basin. *Sci. Bull.* 70, 263–272. doi:10.1016/j.scib.2024.07.007

Tu, K., Ye, S., Zou, J., Hua, C., and Guo, J. (2023). InSAR displacement with high-resolution optical remote sensing for the early detection and deformation analysis of active landslides in the upper yellow river. *Water* 15, 769. doi:10.3390/w15040769

Ullah, M., Tang, B., Huangfu, W., Yang, D., Wei, Y., and Qiu, H. (2024). Machine learning-driven landslide susceptibility mapping in the himalayan China–Pakistan economic corridor region. *Land* 13, 1011. doi:10.3390/land13071011

Valenzuela, P., Domínguez-Cuesta, M. J., García, M. A. M., and Jiménez-Sánchez, M. (2017). A spatio-temporal landslide inventory for the NW of Spain: BAPA database. *Geomorphology* 293, 11–23. doi:10.1016/j.geomorph.2017.05.010

Wang, H., Pan, D., and Jin, Y. (2015). Contributing rate of slope gradient to landslide growth in Qianjiang District of Chongqing. *J. Chongqing Jiaot. Univ. Sci.* 33, 81–84. (in Chinese). doi:10.3969/j.issn.1674-0696.2014.05.18

Wang, P., Li, L., Xu, C., Zhang, Z., and Xu, X. (2022). An open source inventory and spatial distribution of landslides in Jiyuan City, Henan Province, China. *Nat. Hazards Res.* 2, 325–330. doi:10.1016/j.nhres.2022.10.004

Wang, Q., Xu, C., and Xu, J. (2024a). Exploration of landslide geomorphology and inventory construction in Minhe county, Qinghai, China, based on Google Earth remote sensing imagery. *Trans. GIS* 29. doi:10.1111/tgis.13281

Wang, T., Wu, S. R., Shi, J. S., Xin, P., and Wu, L. Z. (2018). Assessment of the effects of historical strong earthquakes on large-scale landslide groupings in the Wei River midstream. *Eng. Geol.* 235, 11–19. doi:10.1016/j.enggeo.2018.01.020

Wang, W., Huang, Y., and Li, l. (2021). Development and distribution of ancient landslides in the northwest corner of the Tibetan Plateau. *IOP Conf. Ser. Earth Environ. Sci.* 861, 052034. doi:10.1088/1755-1315/861/5/052034

Wang, W., Huang, Y., Xu, C., Shao, X., Li, L., Feng, L., et al. (2024b). Identification and distribution of 13003 landslides in the northwest margin of Qinghai-Tibet Plateau based on human-computer interaction remote sensing interpretation. *China Geol.* 7, 171–187. doi:10.31035/cg2023140

Wang, Z., Hu, Z., Liu, H., Gong, H., Zhao, W., Yu, M., et al. (2010). "Application of the relief degree of land surface in landslide disasters susceptibility assessment in China," in *2010 18th international conference on geoinformatics*, 1–5.

Wei, Z., Cao, X., Zhang, J., Ying, Z., Yan, H., and Wei, S. (2021). Temporal and spatial characteristics of landslide, rockfall and debris flow disasters in Qinghai Province during the period. *Chin. J. Geol. Hazard Control* 32, 134–142. (in Chinese). doi:10.16031/j.cnki.issn.1003-8035.2021.06-16

Wieczorek, G. F. (1984). Preparing a detailed landslide-inventory map for hazard evaluation and reduction. *Bull. Assoc. Eng. Geol.* 21, 337–342. doi:10.2113/gseegeosci.xxi.3.337

Wu, X., Xu, X., Yu, G., Ren, J., Yang, X., Chen, G., et al. (2024). The China active faults database (CAFD) and its web system. *Earth Syst. Sci. Data* 16, 3391–3417. doi:10.5194/essd-16-3391-2024

Wu, Y., Dong, Y., Wei, Z., Dong, J., Peng, L., Yan, P., et al. (2023). Genetic mechanisms and a stability evaluation of large landslides in Zhangjiawan, Qinghai Province. *Front. Earth Sci.* 11, 1140030. doi:10.3389/feart.2023.1140030

Xia, G., Liu, C., Xu, C., and Le, T. (2021). Dynamic analysis of the high-speed and long-runout landslide movement process based on the discrete element method: a case study of the shuicheng landslide in guizhou, China. *Adv. Civ. Eng.* 2021, 8854194. doi:10.1155/2021/8854194

Xiao, Z., Xu, C., Huang, Y., He, X., Shao, X., Chen, Z., et al. (2023). Analysis of spatial distribution of landslides triggered by the Ms 6.8 Luding earthquake in China on September 5, 2022. *Geoenvironmental Disasters* 10, 3. doi:10.1186/s40677-023-00233-w

Xie, C., Huang, Y., Li, L., Li, T., and Xu, C. (2023). Detailed inventory and spatial distribution analysis of rainfall-induced landslides in Jiexi County, Guangdong Province, China in August 2018. *Sustainability* 15, 13930. doi:10.3390/su151813930

Xin, P., Dong, X., Wu, S., Shi, J., Wang, T., and Liang, C. (2017). The accumulation characteristics and mechanism of rotational-translational landslides in the Neogene basins on the northeastern margin of Tibet Plateau. *Acta Geol. Sin.* 91, 499–509. doi:10.1016/j.enggeo.2018.07.024

Xu, C. (2015). Preparation of earthquake-triggered landslide inventory maps using remote sensing and GIS technologies: principles and case studies. *Geosci. Front.* 6, 825–836. doi:10.1016/j.gsf.2014.03.004

Xu, C., Xu, X., Yao, X., and Dai, F. (2014). Three (nearly) complete inventories of landslides triggered by the May 12, 2008 Wenchuan Mw 7.9 earthquake of China and their spatial distribution statistical analysis. *Landslides* 11, 441–461. doi:10.1007/s10346-013-0404-6

Xu, L., and Yan, D. (2019). The groundwater responses to loess flowslides in the Heifangtai platform. *Bull. Eng. Geol. Environ.* 78, 4931–4944. doi:10.1007/s10064-018-01436-4

Xu, Y., Guo, W., Wang, W., Luo, S., Chen, Z., Lou, Y., et al. (2022). Characteristics of shallow landslides under extreme rainfall and their effects on runoff and sediment on the Loess Plateau. *Acta Ecol. Sin.* 42, 7898–7909. doi:10.5846/stxb202110313052

Xue, Z., Xu, C., Gao, H., and Huang, Y. (2023). Disaster chain thinking improves the capabilities of disaster prevention, mitigation, and relief in China. *Nat. Hazards Res.* 4, 320–323. doi:10.1016/j.nhres.2023.11.013

Yin, Y., Wang, H., Gao, Y., and Li, X. (2010a). Real-time monitoring and early warning of landslides at relocated wushan Town, the three gorges reservoir, China. *Landslides* 7, 339–349. doi:10.1007/s10346-010-0220-1

Yin, Z., Wei, G., Qi, X., and Zhou, C. (2010b). Preliminary study on characteristic and mechanism of super-large landslides in Upper Yellow River since late-pleistocene. *J. Eng. Geol.* 18, 41. (in Chinese). doi:10.3969/j.issn.1004-9665.2010.01.006

Zhang, M., and Liu, J. (2010). Controlling factors of loess landslides in western China. *Environ. Earth Sci.* 59, 1671–1680. doi:10.1007/s12665-009-0149-7

Zhang, S., Sun, P., Li, R., and Wang, F. (2023). Preliminary investigation on a catastrophic loess landslide induced by heavy rainfall on 1 September 2022 in Qinghai, China. *Landslides* 20, 1553–1559. doi:10.1007/s10346-023-02086-8

Zhang, X., Xu, C., Li, L., Feng, L., and Yang, W. (2024). Inventory of landslides in the northern half of the Taihang mountain range, China. *Geosciences* 14, 74. doi:10.3390/geosciences14030074

Zhang, Y., Guo, C., Lan, H., Zhou, N., and Yao, X. (2015). Reactivation mechanism of ancient giant landslides in the tectonically active zone: a case study in Southwest China. *Environ. Earth Sci.* 74, 1719–1729. doi:10.1007/s12665-015-4180-6

Zhao, B., Su, L., Xu, Q., Li, W., Xu, C., and Wang, Y. (2023). A review of recent earthquake-induced landslides on the Tibetan Plateau. *Earth-Science Rev.* 244, 104534. doi:10.1016/j.earscirev.2023.104534

Zhao, D., Lancuo, Z., Hou, G., Xu, C., and Li, W. (2021). Assessment of geological disaster susceptibility in the hehuang valley of Qinghai province. *J. Geomechanics* 27, 83–95. (in Chinese). doi:10.12090/j.issn.1006-6616.2021.27.01.009

Zhao, J., Huang, Q., Peng, J., Wang, Z., Ma, P., Leng, Y., et al. (2025). Typical characteristics and causes of giant landslides in the upper reaches of the Yellow River, China. *Landslides* 22, 313–334. doi:10.1007/s10346-024-02363-0

Zhao, J., Xu, C., and Huang, X. (2024). Detailed landslide traces database of hancheng county, China, based on high-resolution satellite images available on the Google Earth platform. *Data* 9, 63. doi:10.3390/data9050063

Zhou, B., Zhang, Y. X., Sun, Y., and Gan, C. P. (2013). Study on failure mechanism and stability of loess slope in Huangshui River Basin. *Appl. Mech. Mater.* 405, 580–586. doi:10.4028/www.scientific.net/amm.405-408.580

Zhou, J., Zhu, C., Zheng, J., Wang, X., and Liu, Z. (2002). Landslide disaster in the loess area of China. *J. For. Res.* 13, 157–161. doi:10.1007/bf02857244